Electron Collection by an Electrodynamic Bare Tether at High Potential

by

Jean-Benoît Ferry

Submitted to the Department of Aeronautics and Astronautics
in partial fulfillment of the requirements for the degree of

Master of Science in Aeronautics and Astronautics

at the

MASSACHUSETTS INSTITUTE OF TECHNOLOGY

June 2003

Author .....
Department of Aeronautics and Astronautics
May 23, 2003

Certified by .....
Manuel Martinez-Sanchez
Professor
Thesis Supervisor

Accepted by .....
Edward M. Greitzer
H.N. Slater Professor of Aeronautics and Astronautics
Chair, Committee on Graduate Students

Electron Collection by an Electrodynamic Bare Tether at High Potential

by

Jean-Benoît Ferry

Submitted to the Department of Aeronautics and Astronautics
on May 23, 2003, in partial fulfillment of the
requirements for the degree of
Master of Science in Aeronautics and Astronautics

Abstract

In tethered satellites, it is very important to be able to estimate the electron current collected by the tether. However, this analysis is very difficult because of the presence of the geomagnetic field. We are developing a Particle-In-Cell model. The model uses a boundary condition based on quasi-neutrality, very similar to the one T. Onishi used in his Ph.D Thesis (2002), in order to solve for the local potential at the points of the computational boundary. This condition imposes ne = ni at the boundary. Moreover the motion of particles is computed analytically in a domain close to the tether - inside the sheath. This calculation is made possible by neglecting the space charge effect, which is very small in comparison with the tether potential, and therefore allowing the Laplace equation to be solved. The goal of this analytical domain is to provide a better accuracy in the region where electrons can reach high velocity. Although a similar approach was used by T. Onishi, the goal of this model is to experiment higher voltages for the tether, with bias ratio of the order of 1000 to 2500. Indeed such voltages are the ones of interest for space tethers. In order to be able to reach these voltages, we first conducted a precise analysis of the quiescent un-magnetized case. This analysis allowed us to successfully compare the model with established probe theory results. Moreover it gives a good foundation to explore the more complicated case of a magnetized flowing plasma.

Thesis Supervisor: Manuel Martinez-Sanchez
Title: Professor

Acknowledgments

The realisation of this thesis was a long journey. Without the help of many people, I would have never seen the end of the road.

First of all I want to thank my parents: they always helped me find the right path, and they always supported me when choices were tough to make.
I am also grateful to my advisor, Professor Martinez Sanchez, he was always comprehensive and available when I needed advice. Thanks also to Tatsuo, he helped me very patiently in understanding his huge work on space tethers.
Of course this would not have been possible without my officemates, Luís and Murat. They know how to turn a sunless office into a bright and happy place.

Last but no least, Nathalie was always here when I needed courage and strength. She always had a smile for me. My stay at MIT would not have been the same without the warmth of her love.

Contents

List of Figures

List of Tables

Chapter 1

Introduction

1.1 Electrodynamic Space Tethers

When a tether is made out of a conductive material and placed in a magnetic field, it can be used to produce a Lorenz Force by driving a current in it. Moreover if this tether is attached to a spacecraft, it can be used, either to produce thrust or drag. In the first case, it needs to be powered, whereas in the second case, the tether itself will produce an induction current. This kind of device can be used for de-orbiting or for re-boosting.

The result is that tethers are very attractive for several reasons: first of all, they can be used for both power and thrust generation, contrarily to other propulsion devices. Moreover electrodynamic space tethers are propellantless, which allows to get rid of one of the most critical earth dependency issue - propellant resupply: usually it is possible for a spacecraft to generate its own power, but it is impossible to generate propellant. And finally propellantless re-boost also means exhaustless re-boost, with no risk of contamination or damage on the spacecraft exterior surface.

1.2 Mechanism

1.2.1 Thrust generator

As we previously saw, a tether can be used in two different modes. Let us consider the case of a thruster. If a potential is applied at one end of the tether, a current loop is created. This current loop contains several parts. The most obvious one is the tether itself with a power generator at one end. What is less clear is how this loop is closed. This is actually done by using the ambient ionospheric plasma: First, electrons are collected by the tether, because of its high potential. Then, they are driven through the tether up to the power generator. And finally those electrons are sent back to the plasma by a small device, like an electron gun, in order to neutralize the spacecraft. The result of this process is a Lorenz force created by the current circulating into the tether. This force is given by:

$$\mathbf{F} = \int_0^L j \cdot \mathbf{dl} \times \mathbf{B} \tag{1.1}$$

As a consequence, we can see that one of the driving parameters for the thruster is the intensity of the current. Therefore it is very important to better understand how electrons are collected. Indeed this is the limiting factor to how much current it is possible to generate in order to get thrust out of this space propulsion device. The aim of this thesis is to provide numerical models that allow a better understanding of the physics of the phenomenon and to predict what can be the performances of electrodynamic bare tethers in term of collected current.

1.2.2 Power generator

Space tethers can also be used as power generators, which make them the only one space propulsion device that is fully reversible. In the case of a power generator, we have the following. The motion of the current loop in the geo-magnetic field is creating an induced current. This current in turn, will create a Lorenz force in the direction opposed to the motion. This tells us that conservation of energy is satisfied:

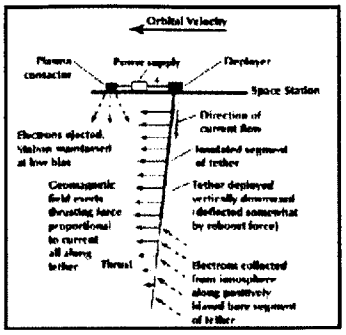

Figure 1-1: A spacecraft with an Electrodynamic Tether

the kinetic energy of the spacecraft is converted into electrical work.

The consequence of this is that if one needs to slow down a spacecraft, by using an electrodynamic tether, one can get electric power from the operation, instead of just wasting the kinetic energy stored into the spacecraft.

Chapter 2

Previous work

2.1 Orbital Motion Limit

2.1.1 Definition

The Orbital Motion Limit provides a maximum for the amount of current which can be collected by a conductive tether. The notion was first introduced by Langmuir and Mott-Smith and is fundamental for the understanding of conductive bare tethers. OML applies when there are no potential barriers preventing an electron coming from infinity to be collected. When this regime applies, it is relatively easy to compute the current collected by a tether. Sanmartin and Estes [1] did it as follows: in a collisionless plasma, the distribution of electrons must be Maxwellian:

$$f(v) = n_\infty(\frac{m_e}{2\pi kT_e})^{3/2}\exp(-\frac{\frac{m_e}{2}(v_r^2+v_\theta^2+v_z^2)-e\phi}{kT_e}) \tag{2.1}$$

Therefore by a change of variable:

$$E = \frac{m_e}{2}(v_r^2+v_\theta^2+v_z^2)-e\phi \tag{2.2}$$

$$J = mrv_\theta \tag{2.3}$$

We get to the following formulas for the electron density:

$$\frac{n_e}{n_\infty} = \int\int \frac{\exp(-\frac{E}{kT_e})dEdJ}{2\pi kT_e\sqrt{J_r^2(E) - J^2}} \tag{2.4}$$

Where J_r is defined for a given r as:

$$J_r^2 = 2m_e r^2(E + e\phi) \tag{2.5}$$

In order to determine the domain of integration, we introduce:

$$J_r^*(E) = \min(J_r'(E); r \leq r' \leq \infty) \tag{2.6}$$

Then we find that incoming electrons to be counted in the integration are given by $0 \leq J \leq J_r^*(E)$ whereas outgoing electrons should be in the range $J_{r_p}^*(E) \leq J \leq J_r^*(E)$. Finally equation (2.4) can be rewritten as:

$$\frac{n_e}{n_\infty} = \int_0^\infty \frac{dE}{\pi kT_e}\exp(-\frac{E}{kT_e})[2\arcsin\frac{J_r^*(E)}{J_r(E)} - \arcsin\frac{J_{r_p}^*(E)}{J_r(E)}] \tag{2.7}$$

And the current density itself is given by:

$$j = en_\infty\sqrt{\frac{2e\phi_p}{m_e}}\int_0^\infty \frac{dE}{kT_e}\exp(-\frac{E}{kT_e})\frac{J_{r_p}^*(E)}{J_{r_p}^*(0)} \tag{2.8}$$

Finally if we are in the domain of validity of OML, there is no potential barrier. As a consequence: $J_r^*(E) = J_r(E)$ and:

$$j = en_\infty\sqrt{\frac{2e\phi_p}{m_e}} \tag{2.9}$$

$$\frac{n_e(r_p)}{n_\infty} = \frac{1}{2} \tag{2.10}$$

We can see that the OML gives a maximum for the collected current in the case of a quiescent un-magnetized plasma. Indeed it is the case for which all the electrons with enough energy can be traced back to infinity from the surface of the tether,

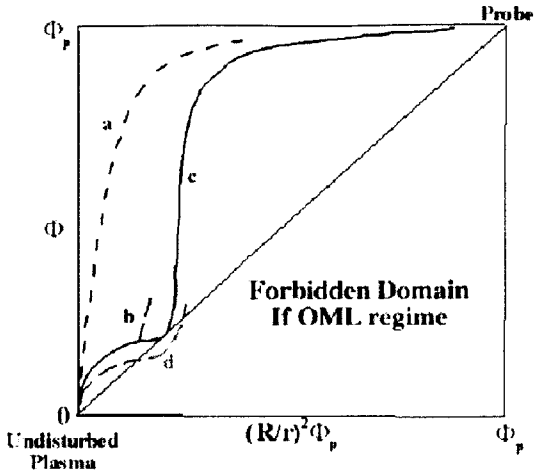

Figure 2-1: Graphical criterion of potential profile for the OML current collection

none of them being returned to the tether by a potential barrier. Tracing the motion forward, this means that electrons will impinge on the tether at all angles, all the way to grazing incidence. Under non-OML conditions there would be a maximum incidence angle, lower than 90°.

2.1.2 Domain of Validity

In their work, Sanmartín and Estes also developed a solution in order for one to know if OML regime is valid or not when $e\phi_p \gg kT_e$. Indeed they noticed that to have $J_r^*(E) = J_r(E)$ for the entire range $0 \leq E < \infty$ it is enough to have $J_r^*(0) = J_r(0)$. Therefore from $J_r^2 \propto r^2\phi(r)$ we get a no potential barrier condition: $r^2\phi(r) \leq r'^2\phi(r'); r \leq r'$

Then the OML condition is given by:

$$\frac{{r_p}^2}{r^2} \leq \frac{\phi(r)}{\phi_p} \tag{2.11}$$

Here,r_p andϕ_p are namely the radius of the tether and its potential. This condition can be conveniently represented by plotting $\frac{\phi}{\phi_p}$ versus $(\frac{r_p}{r})^2$. As it is represented on figure 2-1, if the plot goes below the diagonal of the square, it means that we are not in OML anymore.

2.2 Previous computational works

2.2.1 Laframboise (1966)

In 1966 Laframboise [3] calculated very accurate solutions for current collected by a cylinder and a sphere in a quiescent and unmagnetized plasma. He assumed Maxwellian distribution at infinity and traced enough particles to fill his computational domain. To do so he assumed symmetry in the field quantities and conservation

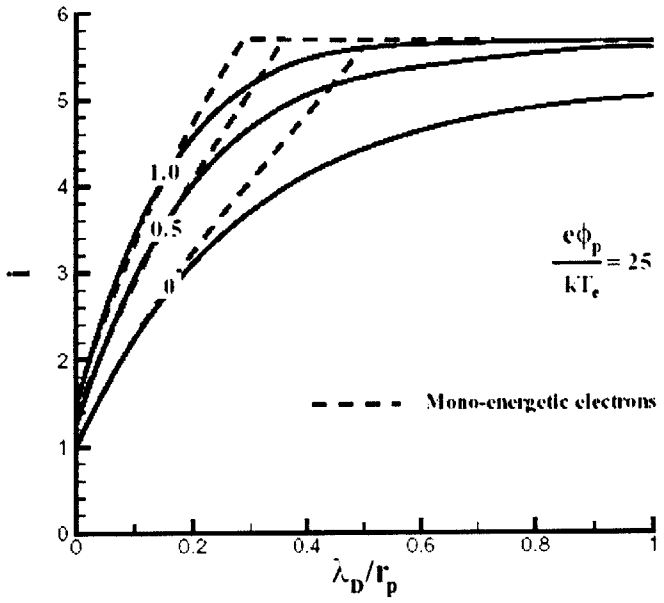

Figure 2-2: Collected current by a cylinder probe

of energy and angular momentum. Since the density of ions in the steady state is derived from a Maxwellian distribution (everywhere except for a negligible cutoff tail due to the presence of the tether) which is independent of mass, the electron/ion mass ratio was not important. Those computations where done for bias ratios up to 25 and for various probe radii. Among those radii, the ones smaller than or of the order of the Debye length gave the OML current collection.

2.2.2 Onishi (1998, 2002)

In is Master's thesis [4], T. Onishi wrote a 2 dimensional PIC code for the symmetric case of a bare tether in a quiescent unmagnetized plasma. In this PIC code the ratio of the mass of the electrons and the mass of the ions was arbitrarily high, since this is of no importance in steady state for potentials of the tether higher than the plasma thermal energy. However the PIC method was not accurate enough for high tether potentials. Indeed in this case the electron velocity gets high enough that they can travel a distance much longer than the size of a cell. As a consequence he could not compute collected current and densities of electrons and ions for a bias ratio higher than 25.

In 2002 in his PhD thesis [5], Onishi developed a new code based on his Master's work. This code was designed to simulate an electrodynamic bare tether in a flowing magnetized plasma. In order to do so he implemented a new grid system (square grid). In addition he introduced a domain close to the tether in which the space charge effect is negligible compared with the influence of the tether and the potential is nearly axi-symmetric. Then, in this domain he was able to compute analytically the motion of the electrons, by using energy and momentum conservations.

A very important point is that for such a case the mass of the ions cannot be chosen arbitrarily: because of their mass, ions are not magnetized and their motion is sub-sonic, whereas electrons are supersonic and magnetized (therefore their motion must be tri-dimensional). This very specific condition is called the meso-thermal condition and can be written as follow:

$$v_T^i \ll U \ll v_T^e \tag{2.12}$$

Where v_T^i and v_T^e are the thermal velocities for ions and electrons (for a given species, $v_T = \sqrt{3kT/m}$), and U is the flow velocity. As a consequence, the simulation process becomes very slow.

Chapter 3

Numerical methods

The numerical method used for this model was a PIC method combined with Analytical motion in a domain close to the tether, where the potential is driven by the tether potential, and where the space charge effect is negligible.

3.1 PIC method

In our case of a space-tether, we are dealing with low density plasma (density of the order of $10^{11}\ m^{-3}$). As a consequence it is a very good approximation to consider our plasma as collisionless. Thanks to this, we can use the "PIC" method. The Particle in Cell Method is a widely used method in simulations of collision-less plasmas. In this method, particles are grouped in super-particles whose parameters are defined to be equal to the the sum of all the parameters of the particles they include. Each super-particle is represented by its position and its velocity. From the position of the super-particles the density of the plasma is extrapolated to each node of the grid. This density is then used in the right hand side of the Poisson equation:

$$\triangle\phi = -\frac{e(n_i - n_e)}{\varepsilon} \tag{3.1}$$

From this equation the potential is calculated at each node of the grid. Then, the electrical field itself is computed thanks to the relation:

$$\mathbf{E} = -\nabla\phi \tag{3.2}$$

The field is then interpolated to the position of each particle in order to compute its acceleration. The acceleration gives the new velocity, which in turn gives the new position.

$$\mathbf{v_{n+1/2}} = \mathbf{v_{n-1/2}} + \frac{q}{m}\mathbf{E}\Delta t \tag{3.3}$$

$$\mathbf{x_{n+1}} = \mathbf{x_n} + \mathbf{v_{n+1/2}}.\Delta t \tag{3.4}$$

A scheme of the algorithm is given on figure 3-1 The main limitation of this method

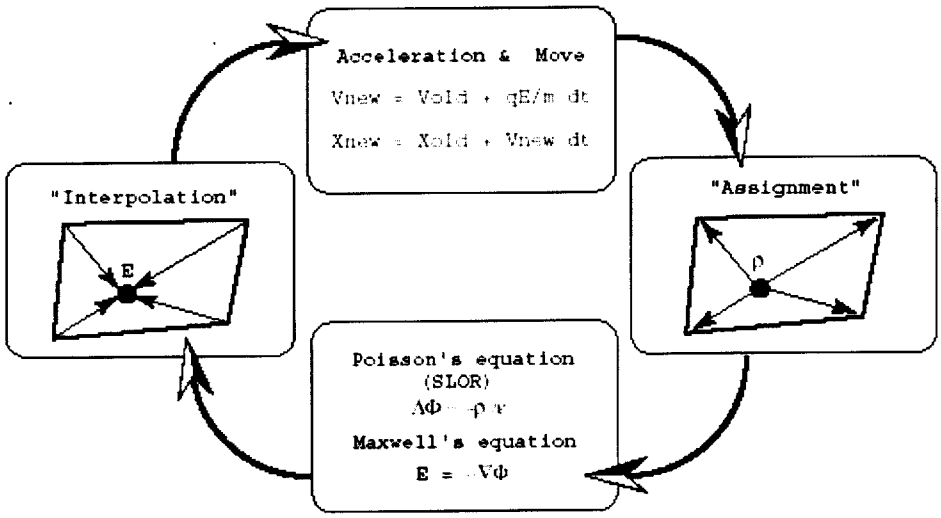

Figure 3-1: The PIC method

is its accuracy. In the case of a very high voltage for the Tether, accelerations become very important and therefore the distance between each position of the particle on the trajectory becomes too big in comparison with the length scale of the system (typically the radius of the tether). The consequences are a trajectory which is no longer smooth and the creation of noise.

Another critical point is the fact that position and velocities are not simultaneous: there is a time-shift of half a time-step between the velocity space and the position space.

3.2 Analytical motion

Inside a small domain around the tether, the calculation of electron motion is done analytically, using conservation of energy and angular momentum. The goal of this analytical domain is to reduce the imprecisions due to the high bias ratio of the tether. In order to be able to solve this problem, we must approximate the potential by a symmetric coulombian potential given by:

$$\phi(r) = \frac{\phi_p \ln(\frac{r}{r_l}) + \phi_l \ln(\frac{r_p}{r})}{\ln(\frac{r_p}{r_l})} \tag{3.5}$$

Where r_p and r_l are namely the radius of the tether and the radius of the analytical domain, and ϕ_p and ϕ_l are the potentials at r_p and r_l. Therefore, the condition for this approximation is that the space charge effect can be neglected in front of the tether effect. We can see that this condition is valid only close to a tether whose bias ratio is high enough, which is precisely where we need to apply it.

Then the conservation laws are:

Conservation of momentum:

$$J = mr^2\dot{\theta} \tag{3.6}$$

Conservation of energy:

$$E = \frac{m}{2}(\dot{r}^2 + r^2 + r^2\dot{\theta}^2) - e\phi(r) \tag{3.7}$$

Combining equations 3.6 and 3.7 gives the following:

$$\dot{r} = \pm\sqrt{\frac{2}{m}(E + e\phi) - \frac{J^2}{m^2r^2}} \tag{3.8}$$

Which, by integration, gives:

$$\Delta t = \pm \int_{r_0}^{r_{new}} \frac{dr}{\sqrt{\frac{2e\phi(r)}{m} - \frac{J^2}{m^2 r^2}}} \tag{3.9}$$

The sign of those equations depends on the sense of the radial motion (inward or outward). Equation 3.9 can be solved for r_{new} at each time step. Then, from the value of r_{new}, it is possible to compute the new value of theta:

$$\Delta\theta = \int_{r_0}^{r_{new}} \frac{Jdr}{r^2 m\sqrt{\frac{2e\phi(r)}{m} - \frac{J^2}{m^2 r^2}}} \tag{3.10}$$

Finally the perigee r_m is determined as being the the radius at which the radial velocity is equal to zero:

$$\frac{2}{m}(E + e\phi) - \frac{J^2}{m^2 r^2} = 0 \tag{3.11}$$

If r_m is found to be lower than r_p, we know that this particular electron is going to be absorbed by the tether.

This method, however, rises an important problem: in the analytical domain, the computation of position and velocity are simultaneous, whereas in the PIC domain, the leapfrog method induce a shift in time between position and velocity. As a consequence, an adjustment is needed, in order to have a smooth transition between the two domain (see figure 3.2).

3.3 Boundary Conditions

The boundary condition for the simulations was based on quasi-neutrality at the boundary of the domain. This condition was represented by:

$$n_e = n_i \tag{3.12}$$

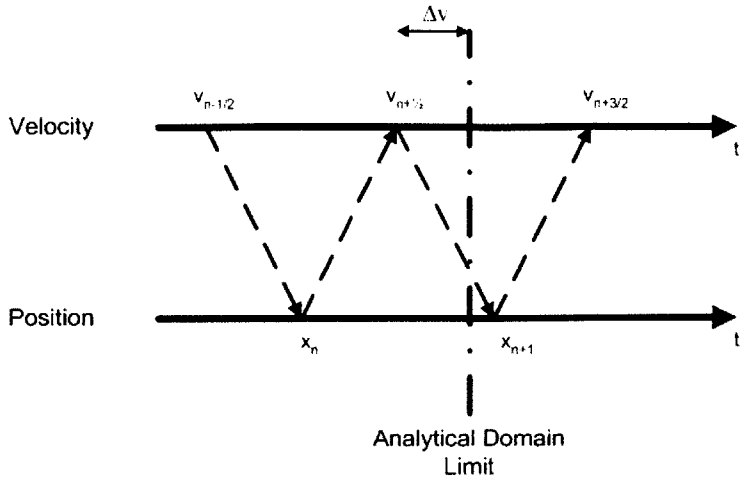

Figure 3-2: The leapfrog method - When a particle enters or exit the analytical domain, because of the shift between velocity and time in the leapfrog method, the velocity must be adjusted

Which can be rewritten, separating the densities of incoming and outgoing particles as:

$$n_e^{in} + n_e^{out} = n_i^{in} + n_i^{out} \tag{3.13}$$

This formulation was then used in a different way depending on wether or not there is flow and magnetic field.

3.3.1 No flow, no magnetic field

Computation of potential at the boundary

In this case, the computation of most of the components of equation 3.13 can be made analytically: the density of incoming ions is given by the integration of a Maxwell-Boltzmann distribution:

$$n_i^{in} = \frac{n_\infty}{2} \exp(-\frac{e\phi}{kT}) \tag{3.14}$$

as well as the density of electrons:

$$n_e^{in} = \frac{n_\infty}{2} \tag{3.15}$$

The outgoing densities are computed from the simulation itself. Finally, the combination of equations 3.13, 3.14 and 3.15 gives an expression for the electric potential at the boundary:

$$\phi_b = -\frac{kT}{e}\ln(1 + 2\frac{n_e^{out} - n_i^{out}}{n_\infty}) \tag{3.16}$$

However the previous equations depend on the assumption that ions are the repelled species and electrons are the attracted one. As a consequence, in order to be consistent, the model should always give a positive potential. Due to the oscillations in the plasma, this is not always the case. That is why when equation 3.16 gives a negative potential, the code assumes that ions are actually attracted and electrons repelled. This is done by exchanging the types of distributions between ions and electrons:

$$n_i^{in} = \frac{n_\infty}{2} \tag{3.17}$$

$$n_e^{in} = \frac{n_\infty}{2}\exp(\frac{e\phi}{kT}) \tag{3.18}$$

This finally leads to the following expression for ϕ_b:

$$\phi_b = \frac{kT}{e}\ln(1 - 2\frac{n_e^{out} - n_i^{out}}{n_\infty}) \tag{3.19}$$

It can be notice that 3.16 and 3.19 are exclusive i.e. it is not possible if the potential was found negative in 3.16 to find it positive in 3.19. This is due to the fact that $\phi_b < 0$ in 3.16 means $n_e^{out} > n_i^{out}$ which in turn gives $\phi_b < 0$ in 3.19.

Injection of new particles

Once the potential at the boundary is known the flux of electrons and ions to be injected is computed analytically:

$$\Gamma_e = \int_{-\infty}^{\infty}\int_{-\pi/2}^{\pi/2}\int_{\sqrt{2e\phi/m_e}}^{\infty} n_\infty(\frac{m_e}{2\pi kT})^{3/2}\exp(-\frac{\frac{1}{2}m_e(w_\perp^2 + w_z^2) - e\phi}{kT})w_\perp^2\cos(\theta)dw_\perp d\theta dw_z \tag{3.20}$$

or

$$\Gamma_e = \frac{n_\infty c_\infty}{4}[\frac{2}{\sqrt{\pi}}\sqrt{\frac{e\phi}{kT}} + \exp(\frac{e\phi}{kT})erfc(\sqrt{\frac{e\phi}{kT}})] \tag{3.21}$$

and for the ions:

$$\Gamma_i = \int_{-\infty}^{\infty}\int_{-\pi/2}^{\pi/2}\int_0^{\infty} n_\infty(\frac{m_i}{2\pi kT})^{3/2}\exp(-\frac{\frac{1}{2}m_i(w_\perp^2 + w_z^2) - e\phi}{kT})w_\perp^2\cos(\theta)dw_\perp d\theta dw_z \tag{3.22}$$

or

$$\Gamma_i = n_\infty(\frac{kT}{2\pi m_i})^{1/2}\exp(-\frac{-e\phi}{kT}) \tag{3.23}$$

Once again if the potential is found to be negative, the expressions for electrons and ions are exchanged.

3.3.2 Case with flow and magnetic field

This case require different boundary conditions for several reasons. First of all in this case, electrons have a 3-D motion because they are magnetized. As a consequence, the condition for an electron to be traced back to infinity can no longer be a 2-D condition. In addition to this, if we consider that the tether is moving in an absolute frame, the conservation of energy cannot be applied anymore.

Derivation of a new condition

If we consider the fact that the tether is now moving, we can derive from Newton's law: (E represents the total energy of an electron in the absolute frame)

$$\frac{dE}{dt} = -eU\frac{\partial\phi}{\partial x} \tag{3.24}$$

Therefore, at a given time t, the condition for an electron to be traced back to infinity is ($v = v_x^2 + v_y^2 + v_z^2$ represents the velocity of an electron in the absolute frame):

$$\frac{1}{2}mv^2 \geq e\phi - \int_{-\infty}^{t} eU\frac{\partial\phi}{\partial x}dt \tag{3.25}$$

Now, considering that we are actually considering an electron far away from the tether, we have $\frac{\nabla\phi}{\phi} \ll r_L$ and it is possible to average quantities over the electrons gyration period. That gives:

$$v_x = 0 \tag{3.26}$$

This yields:

$$\phi = \int_{-\infty}^{t} \frac{d\phi}{dt} dt = \int_{-\infty}^{t} (U\frac{\partial\phi}{\partial x} + v_y\frac{\partial\phi}{\partial y})dt \tag{3.27}$$

Therefore equation 3.25 yields:

$$\frac{1}{2}mv^2 \geq \int_{-\infty}^{t} ev_y\frac{\partial\phi}{\partial y}dt \tag{3.28}$$

This equation means that in an imaginary case in which electrons would only have velocity only on x-axis, the condition for them to be traced back to infinity would be:

$$\frac{1}{2}mv^2 \geq 0 \tag{3.29}$$

A more general interpretation is that the condition on the kinetic energy of an electron should be (at least on the front size of the tether) weaker than being larger to $e\phi$. The next step is to try to figure a coefficient which would take this phenomenon into account.

An easy way to do so is to consider the following approximation: electrons travel on a straight line with a constant velocity on the y axis, potential is a decaying power law. The velocity is assumed to be $\frac{v_{Te}}{\sqrt{3}}$ (Here v_{Te} is the electron thermal velocity: $v_{Te} = \sqrt{3kT_e/m}$). This approximation can be justified as follow:

- Since we are far from the tether, the velocity of electrons did not changed much from there velocity at infinity. This can be written as: $\frac{e\phi_b}{kT} \ll 1$

- The velocity on the y axis (parallel to the magnetic line) can be averaged and is equal to the y-axis contribution to the thermal velocity.

In this case we have the following expression for the potential, where r represents the distance from the tether, and b means "at the boundary":

$$\phi = \frac{\phi_b r_b^\alpha}{r^\alpha} \tag{3.30}$$

Therefore, we can write:

$$\frac{\partial \phi}{\partial y} = \frac{\alpha y \phi_b r_b}{(x^2+y^2)^{1+\alpha/2}} \tag{3.31}$$

Then we know that ($V = \frac{v_{T_e}}{\sqrt{3}}$):

$$x = -\frac{U}{V} \tag{3.32}$$

. This leads to:

$$\frac{\partial \phi}{\partial y} = \frac{\alpha r_b^\alpha \phi_b}{(1+(\frac{U}{V})^2)^{1+\alpha/2}} . \frac{1}{y^{\alpha+1}} \tag{3.33}$$

We can now do the integration:

$$\int_{-\infty}^{t} e v_y \frac{\partial \phi}{\partial y} dt = \frac{e\phi_b}{(1+(\frac{U}{V})^2)^{1+\alpha/2}} . (\frac{r_b}{y_b})^\alpha \tag{3.34}$$

And finally, taking into account the fact that:

$$r_b = y_b \sqrt{1+\frac{U^2}{V^2}} \tag{3.35}$$

We get the following criterion:

$$\frac{1}{2} m v^2 \geq \frac{e\phi_b}{1+(\frac{\sqrt{3}U}{v_{T_e}})^2} \tag{3.36}$$

For the following conditions:

- Power law potential: $\phi \propto \frac{1}{r^\alpha}$
- y-velocity constant for the electrons

The meaning of this algebra is that the thing that really matters in this case is the travel in y-direction.

This provide very important qualitative results. Indeed, it shows that the higher

is the flow velocity, the more chance an electron has to be collected. A physical interpretation for this can be given as follow: for a flow velocity much greater than the thermal velocity of electrons($U \gg v_{T_e}$), electrons are trapped on magnetic lines and there velocity on those lines is so slow that they can be considered as "frozen". Therefore, any electron on the path of the tether will be collected. On the other hand, when electrons have a thermal velocity much higher than the flow velocity ($U \ll v_{T_e}$), there motion can be considered as a 3-D motion, because of their large Larmor radius ($r_L \gg \lambda_D$) and what drives the physics is no longer the magnetic effect.

Densities and potential at the boundary

Using equation 3.36, we can derive a formula for the density of incoming electrons in the same way as we did for the 2-D case. However this time it is not possible to calculate the integrals. This will be done numerically.

$$n_e = \int_0^{\pi} \int_{-\pi/2}^{\pi/2} \int_{\frac{\sqrt{2e\phi/m_e}}{1+(\frac{\sqrt{3}U}{v_{Te}})^2}}^{\infty} n_\infty (\frac{m_e}{2\pi kT})^{3/2} \times \exp(-\frac{\frac{1}{2}m_e((w\cos(\theta)\sin(\psi) - U)^2 + (w\sin(\theta)\sin(\psi))^2 + (w\cos(\psi))^2) - e\phi}{kT}) \times w^2 \sin(\psi) dw d\theta d\psi \tag{3.37}$$

Concerning the ions we can make a 1-D approximation:

$$\frac{1}{2}mw_{x\infty}^2 = \frac{1}{2}mw_x^2 + e\phi_b \tag{3.38}$$

$$\frac{1}{2}mw_{y\infty}^2 = \frac{1}{2}mw_y^2 \tag{3.39}$$

$$\frac{1}{2}mw_{z\infty}^2 = \frac{1}{2}mw_z^2 \tag{3.40}$$

Which leads to the following result:

$$n_i = \int_0^\infty \int_0^\infty \int_{-\pi/2}^{\pi/2} n_\infty (\frac{m_i}{2\pi k T_i})^{3/2} \times \\ \exp(-\frac{(\sqrt{w_\perp^2 \cos(\theta)^2 + 2e\phi} - U)^2 + w_\perp^2 \sin(\theta)^2 + w_z^2}{v_{Ti}^2}) w_\perp dw_z dw_\perp d\theta \tag{3.41}$$

Finally, as explained in subsection 3.3.1, we get the potential at the boundary from the quasi-neutrality condition:

$$n_e^{in} + n_e^{out} = n_i^{in} + n_i^{out} \tag{3.42}$$

Where the outgoing densities are calculated from the previous iteration of the simulation.

Fluxes

Using the same distributions as above and the boundary potential that was just calculated, it is now possible to get an expression for the fluxes of incoming particles, as we did in the no-flow case. Once again, we cannot compute analytically those integrals.

For the electrons we find:

$$\Gamma_e^{in} = \int_0^\pi \int_{-\pi/2}^{\pi/2} \int_{\frac{\sqrt{2e\phi/m_e}}{1+(\frac{\sqrt{3}U}{v_{Te}})^2}}^\infty n_\infty (\frac{m_e}{2\pi k T})^{3/2} \times \\ \exp(-\frac{\frac{1}{2} m_e ((w\cos(\theta)\sin(\psi) - U)^2 + (w\sin(\theta)\sin(\psi))^2 + (w\cos(\psi))^2) - e\phi}{kT}) \times \\ w^3 \cos(\theta) \sin^2(\psi) dw d\theta dw_z \tag{3.43}$$

And for the ions:

$$\Gamma_i^{in} = \int_0^{\infty}\int_0^{\infty}\int_{-\pi/2}^{\pi/2} n_{\infty}(\frac{m_i}{2\pi kT_i})^{3/2}\times \exp(-\frac{(\sqrt{w^2\cos(\theta)^2+2e\phi}-U)^2+w^2\sin(\theta)^2+w_z^2}{v_{Ti}^2})w^2\cos(\theta)dw_z dw d\theta \tag{3.44}$$

However, the ions have such a slow thermal velocity that it is a good approximation to estimate there flux at the front side by a much simpler expression:

$$\Gamma_i^{in} = n_{\infty}U \tag{3.45}$$

Method to accelerate the simulation

In the flow case, it is not possible to simply use ions and electrons with a mass ratio equal to 1. As a consequence, because of the slowness of the ions, it takes a very long time to the simulation before it reaches the steady state. However, there is a way to use lighter ions, without changing the densities of particles, space charge and field. In order to keep the physics unchanged, we simply need to keep two conditions:

- The Mach number for the ions ($\frac{\frac{1}{2}m_iU^2}{kT}$) stays constant
- The meso-thermal condition must remain unchanged: $v_{Ti} \ll U \ll v_{Te}$

If those conditions are satisfied, the non-dimensional quantities driving the ions physics, will remain unchanged. Moreover, the meso-thermal condition being still satisfied, the ions will keep on driving the density of electrons.
Therefore, we can do the following: multiply U by a factor α so that $\alpha U \ll v_{Te}$. Then, once a good alpha is found, we can compute the new mass for ions: m_i/α^2. In this thesis, we used the following value: $\alpha = 5$.

Chapter 4

Nominal case (symmetric)

As explained in the previous chapter for these simulation, a mass ratio equal to one ($\frac{mi}{me} = 1$) was used in order to get faster to the steady state. As a consequence the velocity of ions can be considered as negligible in the derivation of the plasma frequency. Therefore the plasma frequency is found to be:

$$\omega_p = \sqrt{\frac{e^2 n_\infty (m_e + m_i)}{\varepsilon_0 m_e m_i}} = \sqrt{\frac{2e^2 n_\infty}{\varepsilon_0 m_e}} \tag{4.1}$$

4.1 Parameters

The nominal case was designed to represent the conditions in which an electrodynamic space tether could be used, except for the plasma flow and the geomagnetic field. (see table 4.1)

Plasma density	$10^{11}\ m^{-3}$
Plasma temperature	$1160\ K$
Electric charge	$1.6 \times 10^{-19}\ C$
Electron mass	$9.1 \times 10^{-29}\ kg$
Ion mass	$2.672 \times 10^{-25}\ kg$
Debye length	$7.440 \times 10^{-3}\ m$
Plasma time	$5.610 \times 10^{-11}\ s$

Table 4.1: Plasma parameters

The parameters of the tether are the following: $r_p = 1\lambda_D$ and $\phi_p = 25V$

Radius	$1\lambda_D = 7.440 \times 10^{-3}\ m$
Potential	$25\ V$

Table 4.2: Tether parameters

4.2 OML validity

The nominal case is in the OML domain. This is evidenced by the fact that the $\frac{\phi}{\phi_p}$ versus $(\frac{r_p}{r})^2$ plot never crosses the square diagonal:

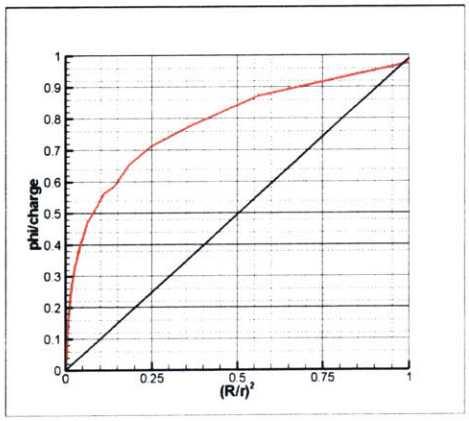

Figure 4-1: $\frac{\phi}{\phi_p}$ versus $(\frac{r_p}{r})^2$

4.3 Current collected

The amount of current collected is as expected equal to the OML current, this is in accordance withe the previous result. The value of OML current in this case is given by equation 2.9. It is found to be $j = 0.0151 A.m^{-2}$ The presence of very periodic oscillations can be observed. The period of these oscillations is found to be equal to the plasma time τ_p. One would expect those oscillation to be damped, but it is not the case. Actually the quasi-neutrality condition at the boundary seems to maintain those oscillation. Indeed experience shows that with a different condition, those oscillations tend to disappear (see section 5.4.2)

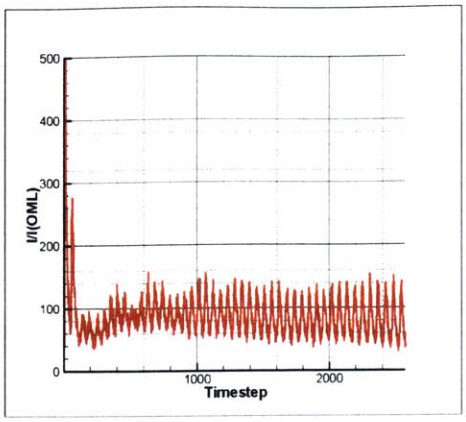

Figure 4-2: Normalized electron collection current (% of OML), $\Delta t = 0.1\frac{\tau_p}{2\pi}$

4.4 Electron density

Figure 4-3 shows a radial representation averaged over 120 time-steps of the electron density. In the domain of validity for OML, the theory tells us that the electron density at the surface of the tether should be $\frac{n_e}{n_\infty} = \frac{1}{2}$. This theoretical result is confirmed by the simulation. There is actually a small overshoot, due to numerical reasons. More precisely this overshoot is probably the consequence of the transition between the numerical and analytical domains.

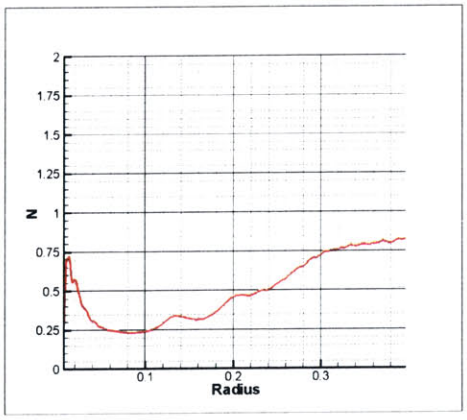

Figure 4-3: Normalized electron density ($\frac{n_e}{n_\infty}$), radius is given in meters

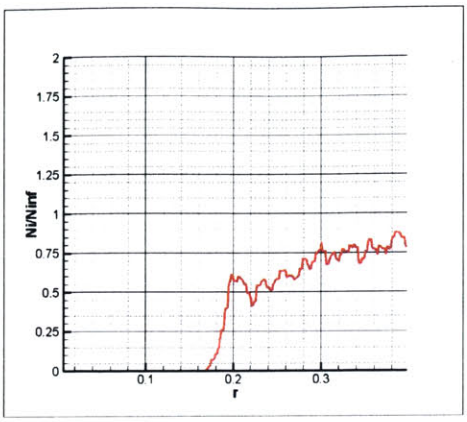

Figure 4-4: Normalized ion density ($\frac{n_i}{n_\infty}$), radius is given in meters

4.5 Ion density

The ions can be very well represented by a Boltzmann distribution, with an exponential decay of the density. Therefore the shape of their density is very stiff. This stiffness make it very convenient to use the ion density in order to define the limit of the sheath.

Chapter 5

Results and Interpretation in the symmetric case

In this chapter we discuss the results for simulations done for three different radius of the tether: 1,3 and 6 Debye length. Finally a comparison with the theoretical models will be done.

5.1 Radius = 1 λ_D

For this radius, the OML applies, and the current collected reaches its theoretical maximum.

5.1.1 OML validity

As it can be seen on figure 5-1, in the case of a tether radius equal to one Debye length ($r_p = 1\lambda_D$), the OML regime is valid. Indeed the plot of $\frac{\phi}{\phi_p}$ versus $(\frac{r_p}{r})^2$ never cross the square diagonal. Therefore, as it is explained in paragraph 2.1.2, the collected current reaches its maximum. This is not always the case when the tether radius is larger.

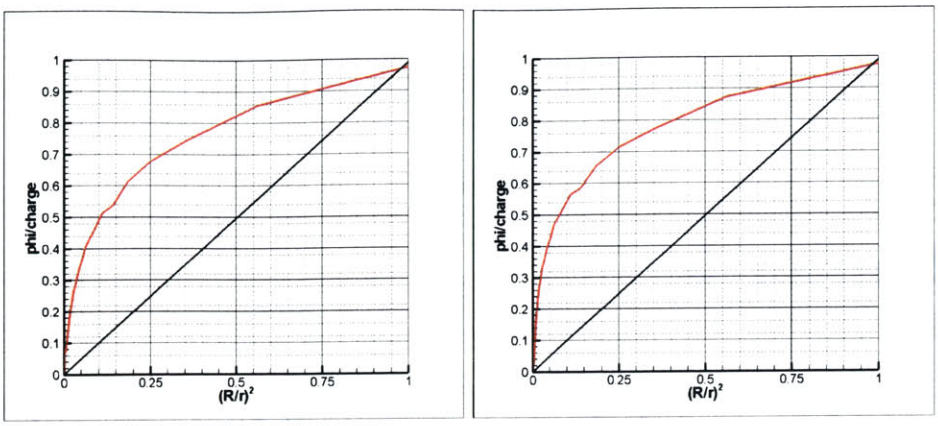

(a) Potential = 10V

(b) Potential = 25V

(c) Potential = 50V

(d) Potential = 100V

Figure 5-1: $\frac{\phi}{\phi_p}$ versus $(\frac{r_p}{r})^2$ for a tether radius equal to $1\lambda_D$.

5.1.2 Electron density

Figure 5-2 shows the electron density for various tether potentials. Several observations can be made: on its value at the tether, and on its shape.

- Value at the tether:

  The theoretical results given in section 2.1.1 give a $\frac{n_e}{n_\infty}$ ratio equal to 1/2. Figure 5-2 shows an overshoot, which is probably due to the imprecisions of the transition between the analytical and PIC domains.

- Shape:

  Furthermore, in unpublished work [6], Sanmartín predicted that there should

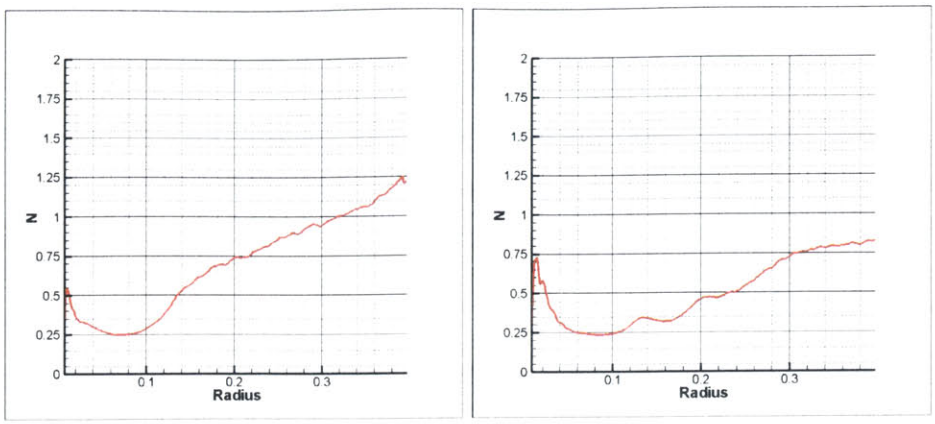

(a) Potential = 10V

(b) Potential = 25V

(c) Potential = 50V

(d) Potential = 100V

Figure 5-2: Normalized electron density for a tether radius equal to $1\lambda_D$

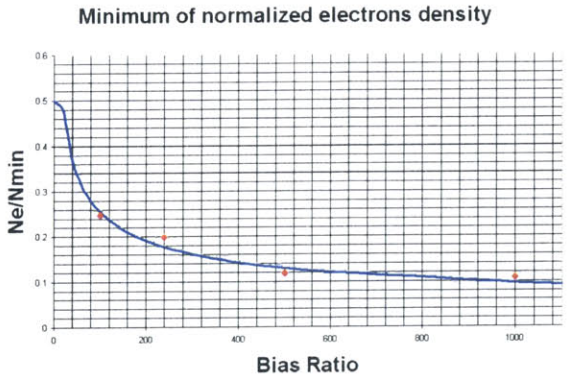

Figure 5-3: The plain line represents the theoretical value of the minimum of the electron density [6], the dots represent the results of the simulation.

be a minimum in electron density which should be lower than the density at the tether. This minimum depends heavily on the variation of the tether bias ratio. The result we got using the PIC simulations confirm this theory. Moreover the value we obtained are very closed to the one expected (see figure 5-3).

5.1.3 Ion density

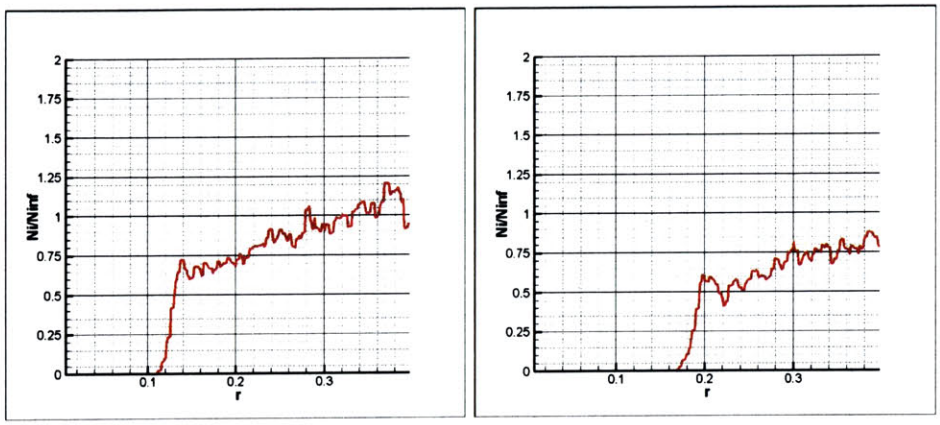

(a) Potential = 10V

(b) Potential = 25V

(c) Potential = 50V

(d) Potential = 100V

Figure 5-4: Normalized ion density for a tether radius equal to $1\lambda_D$

The ion density can be modelled by a Maxwell Boltzman distribution therefore the drop in density of ions is very stiff as it can be seen on figure 5-4 and it can be used to define the limit of the sheath, even if the actual definition of the sheath is the area where the quasi-neutrality is violated. That means in particular that one must

be very cautious when examining the $100V$ case. Indeed it shows that the sheath extends beyond the limit of the computational domain, which is not coherent with the quasi-neutrality boundary condition.

It was noticed that this distance is also the location where $\phi(r)/\phi_p$ presents a hump. This can hardly be noticed on the scale of figure 5-1 but figure 5-5 presents an enlarging for one of the cases (potential equals 25 V).

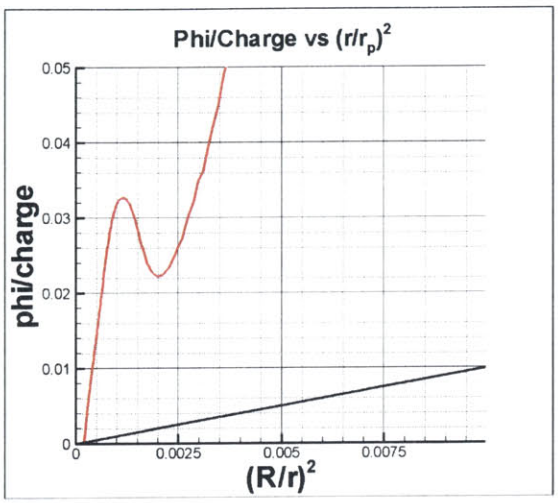

Figure 5-5: $\frac{\phi}{\phi_p}$ versus $(\frac{r_p}{r})^2$ for a tether potential equal to 25 V and a radius equal to $1\lambda_D$

5.1.4 Collected current

For a tether radius equal to $1\lambda_D$ figure 5-1 shows that OML is valid. The amount of current collected confirms this affirmation. Indeed the averaged current is equal to 100% of OML current. However it must be noticed that the current collected oscillates with a constant period: a frequency analysis shows a frequency of oscillation equal to the plasma frequency (f_p). The results are shown on figure 5-6. For a potential equal to 100 V, we are slightly under the OML current (around 80%). This is probably due to the fact that in this case, as explained in section 5.1.3, the sheath extends further than the computational domain, and therefore the boundary condition does not represents the right condition.

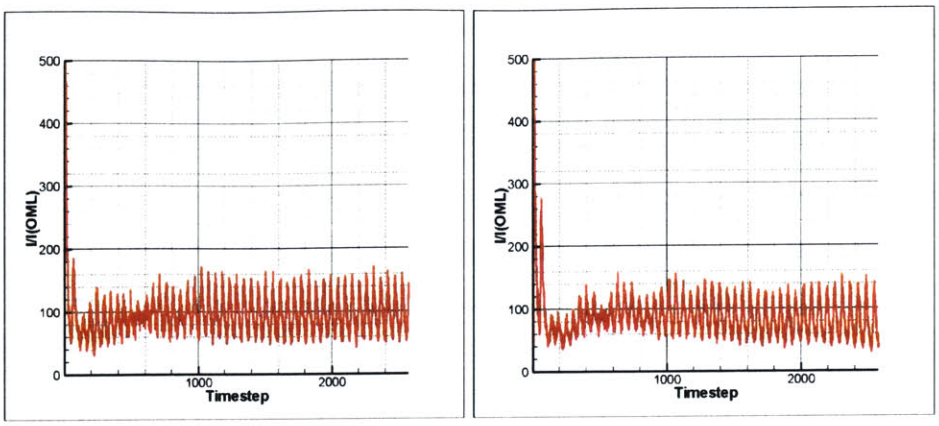

(a) Potential = 10V

(b) Potential = 25V

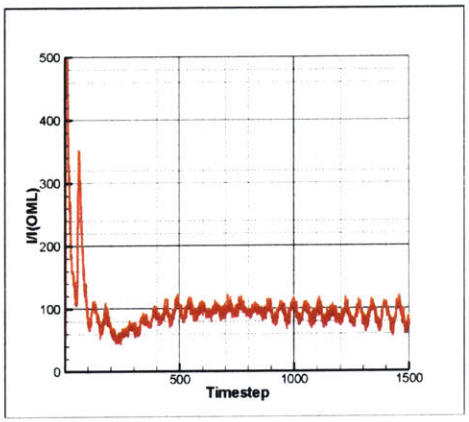

(c) Potential = 50V

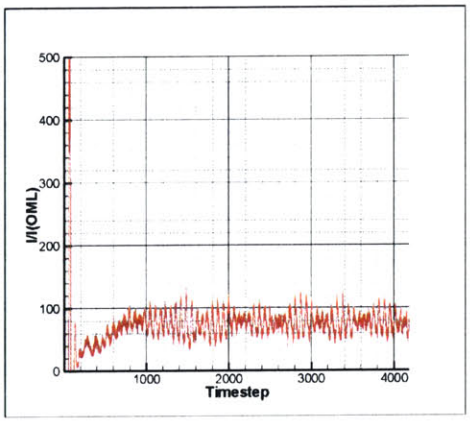

(d) Potential = 100V

Figure 5-6: Current collected (% of OML current) for $r_p = \lambda_D$

This shows that the ratio I/I_{OML} does not depend on the potential of the tether. However the current itself depends on the potential: $I \propto \sqrt{\phi_p}$.

5.2 Radius = 3 λ_D

After investigating the case of a radius equal to $1\lambda_D$, the author switched to cases with larger radii, which are out of the OML domain. Here, we will examine the $3\lambda_D$ radius case for various potentials.

5.2.1 OML validity

In this case the $\frac{\phi}{\phi_p}$ versus $(\frac{r_p}{r})^2$ plots of figure 5-7 show that we are at the boundary of OML validity. On the pictures on the left hand side are full representations of the plot on the $[0,1] \times [0,1]$ square, whereas pictures on the right hand side are enlarging, close to (0, 0). Thus figures 5-7 a, b, c and d show that for potentials lower than 25 volts we are in the OML region but figures 5-7 e and f show that for a potential equal to 50 volts, we are out of the OML regime. Indeed, the plot crosses the diagonal.

5.2.2 Electron density

The electron density gives a lot of information. First of all, we can see that the electron density at the tether is slightly lower than $\frac{1}{2}$. This indicates the presence of potential barriers, whose effect is to prevent some electrons to reach the tether, even if they have enough energy. This phenomenon is a consequence of the theory explained in section 2.1.1. It shows that there is a lack of accuracy in the results of figure 5-7, because the presence of a potential barrier is not compatible with OML. The minimum of the electron density is also lower than the one we got in the $r = 1\lambda_D$ case and the sheath is larger. Both were expected.

5.2.3 Current collected

As expected in the theoretical model given by Sanmartin and Estes, the current collected is lower than the OML current. This is due to the fact that there is an effective potential barrier: it prevents electrons that would be collected otherwise to reach the tether. (figure 5-9). Thus we get a current collected equal to around 80% of the OML current.

It is important here to consider the fact that we are not talking about the current itself but actually about the I/I_{OML} ratio. That is why we get a ratio for the $3\lambda_D$ case lower than the one for the $1\lambda_D$ case. The actual current is higher. Indeed the OML current is directly proportional to the collecting surface. That means that we have: $I(3\lambda_D) = 2.4 \times I(1\lambda_D)$.

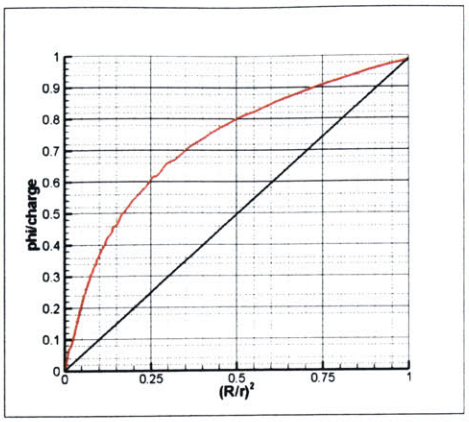

(a) Potential = 10V

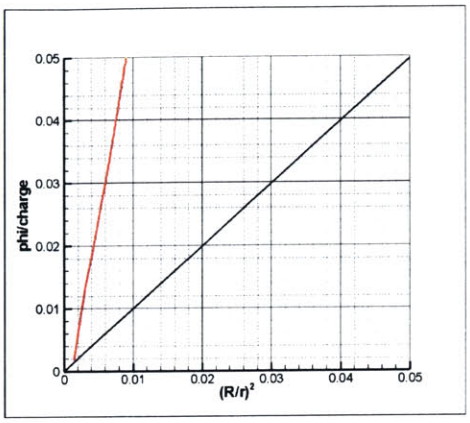

(b) Potential = 10V

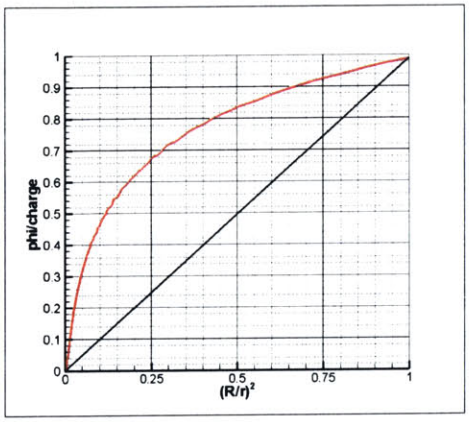

(c) Potential = 25V

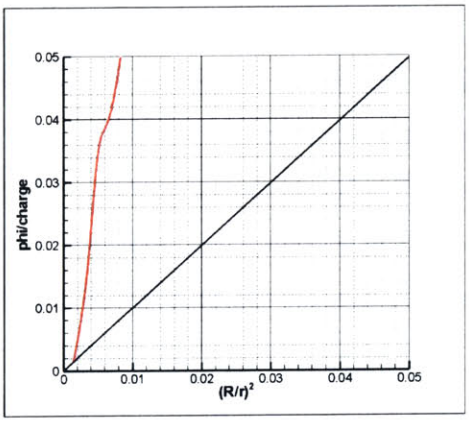

(d) Potential = 25V

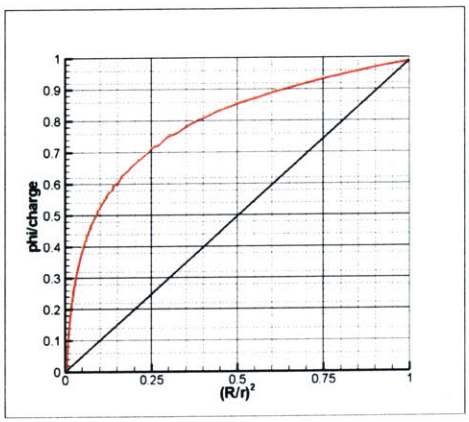

(e) Potential = 50V

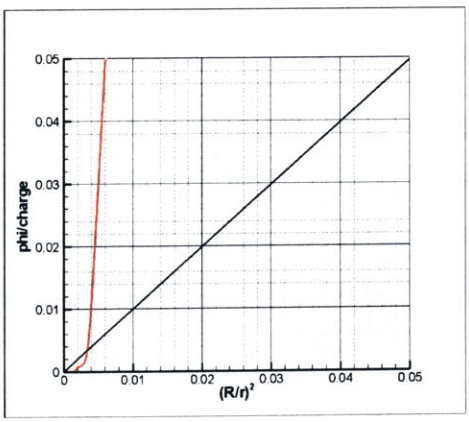

(f) Potential = 50V

Figure 5-7: ϕ/ϕ_p versus $(r_p/r)^2$ for the case $r_p = 3\lambda_D$

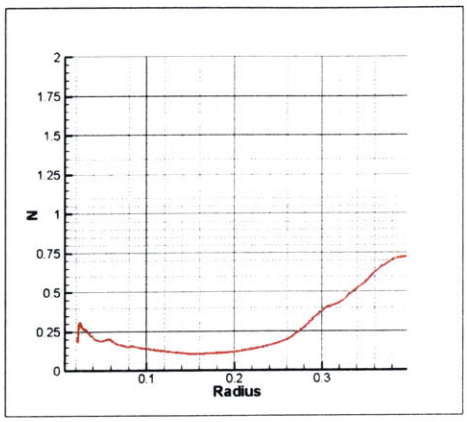

(a) Potential = 10V

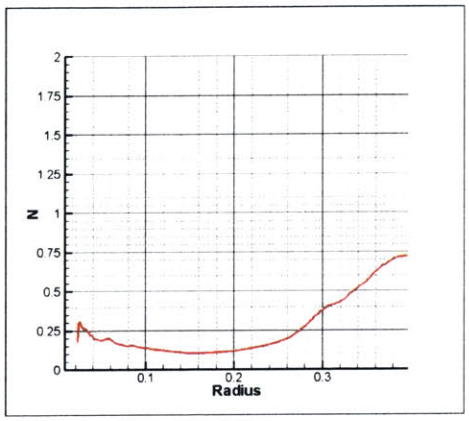

(b) Potential = 25V

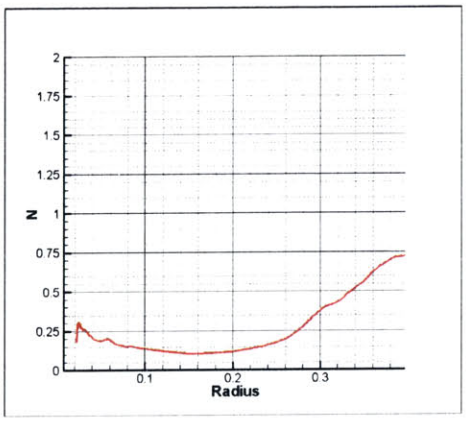

(c) Potential = 50V

Figure 5-8: Normalized electron density for the case $r_p = 3\lambda_D$

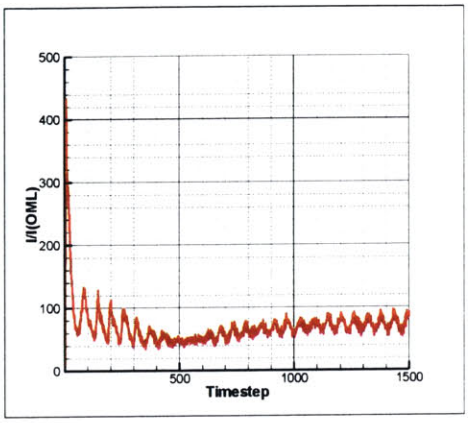

(a) Potential = 10V

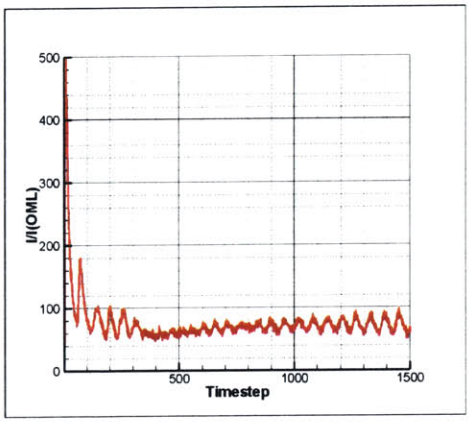

(b) Potential = 25V

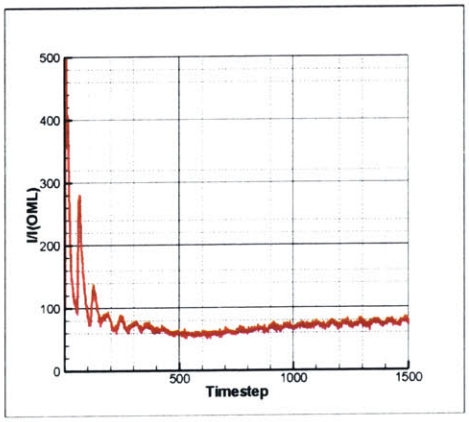

(c) Potential = 50V

Figure 5-9: Current collected for the case $r_p = 3\lambda_D$

5.3 Radius = 6 λ_D

The largest case explored was for a radius equal to $6\lambda_D$. In this case, we are clearly out of the OML region and this is confirmed by all the variables.

5.3.1 OML Validity

The $\frac{\phi}{\phi_p}$ versus $(\frac{r_p}{r})^2$ plots of figure 5-10 clearly show that we are not in the domain of validity of OML, for any voltage of the tether.

5.3.2 Electron Density

The electron density (figure 5-11) confirms the fact that we are out of the OML regime. Moreover the minimum of density is lower than in the previous cases and much flatter. This is due to the increase in the size of the sheath. Actually, the sheath is now very far away from the tether, and its limit is well out of the computational domain.

5.3.3 Current collected

Once again the normalized collected current is lower than the OML current. (figure 5-12)

5.4 Discussion

5.4.1 Size of the sheath

The size of the sheath is theoretically highly dependant on the bias ratio of the tether. It can be proven that the dependency is given by the following relation (r_s is the size of the sheath):

$$r_s \propto (\frac{e\phi_p}{kT})^{3/4}\lambda_D \tag{5.1}$$

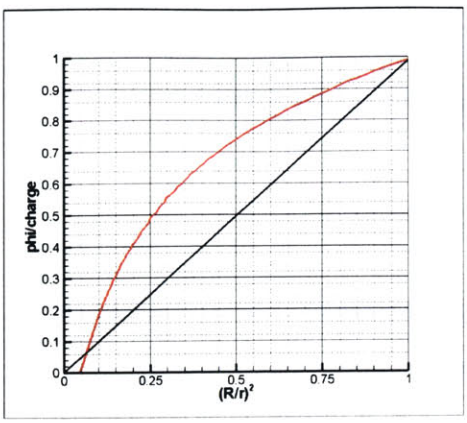

(a) Potential = 10V

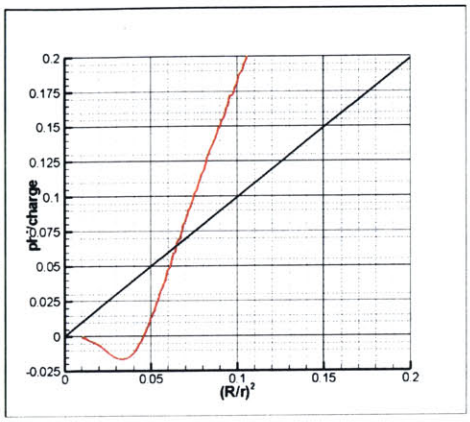

(b) Potential = 10V

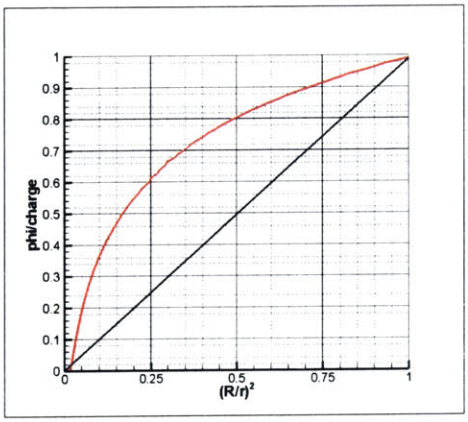

(c) Potential = 25V

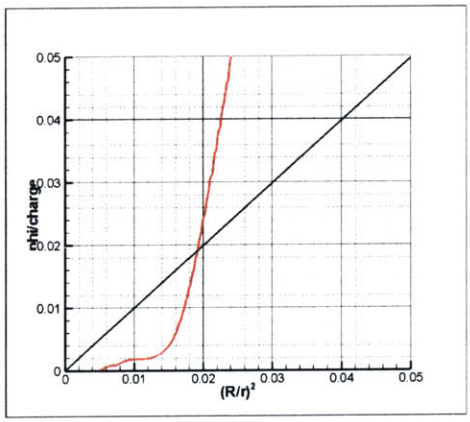

(d) Potential = 25V

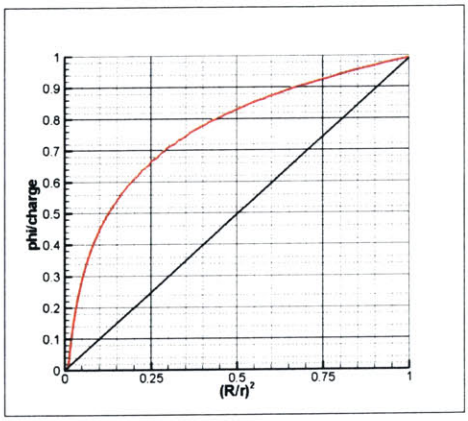

(e) Potential = 50V

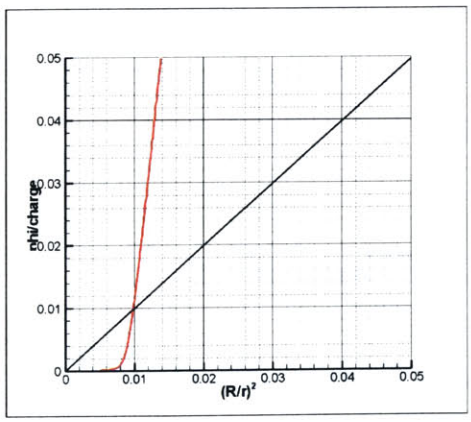

(f) Potential = 50V

Figure 5-10: OML validity check for the case $r_p = 6\lambda_D$

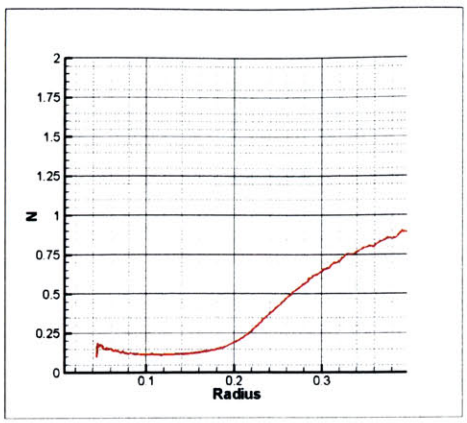

(a) Potential = 10V

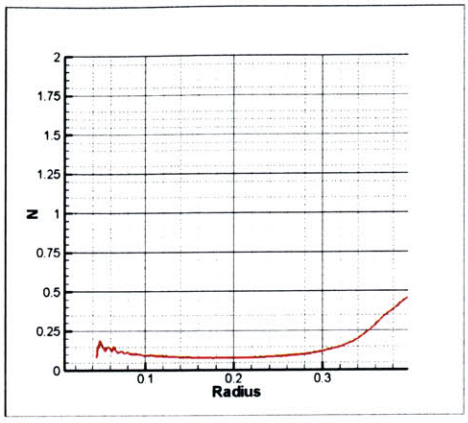

(b) Potential = 10V

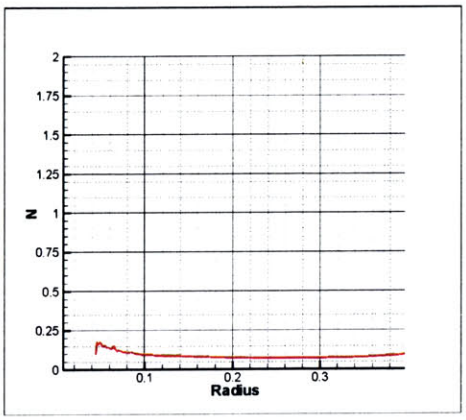

(c) Potential = 50V

Figure 5-11: Electron density for the case $r_p = 6\lambda_D$, the radius is given in meters

That is why it is interesting to plot r_s versus $(\frac{e\phi_p}{kT})^{3/4}$. This was done on figure 5-13. We can see that the relation we get is nearly linear, confirming the theoretical results. Unfortunately, because of the limited size of the computational domain, the author could not get the size of the sheath of the case with bigger radii, for voltages higher than 50V. Indeed, the limit of the sheath was out of the boundary.

The transition between the sheath and the non-sheath region is also observed on the $\frac{\phi}{\phi_p}$ versus $(\frac{r_p}{r})^2$ plots. It occurs where $r^2\phi(r)$ reaches a minimum. Indeed below this point, the two following conditions apply:

- $J_r^\star(E) = J_r(E)$ (see section 2.1.1 for definitions)
- $n_e \approx n_i$

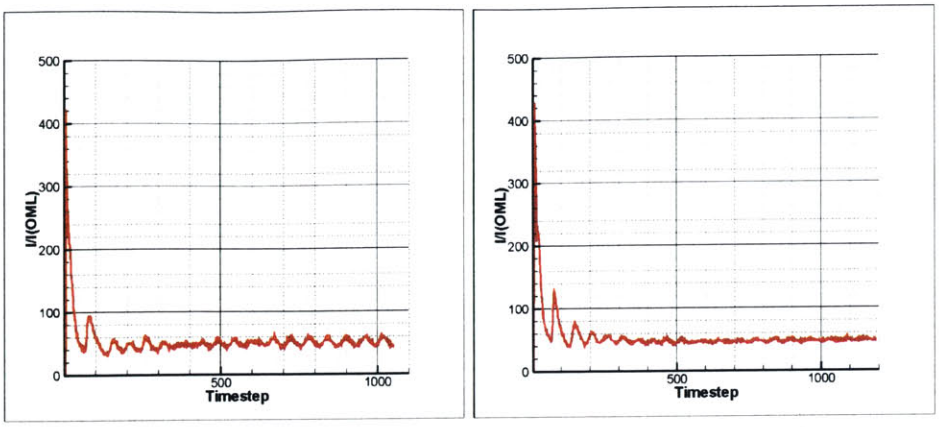

(a) Potential = 10V

(b) Potential = 25V

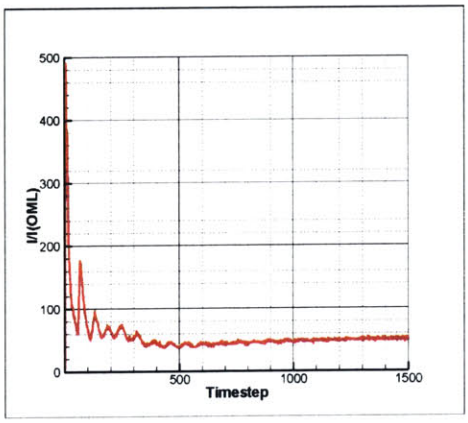

(c) Potential = 50V

Figure 5-12: Current collected (% of OML) for the case $r_p = 6\lambda_D$

Indeed those two conditions lead, by using equation 2.7 and a Maxwellian distribution for the ions:

$$\phi \propto \frac{1}{r} \tag{5.2}$$

5.4.2 Boundary condition

During the various simulation the author tried different models for the calculation of the boundary conditions. It turns out that the use of a constant potential equal to 0 on the boundary does not make a big difference compared to the condition explained in section 3.3. This comes from the fact that the boundary is very far from the tether. Therefore the potential at the boundary is very low.

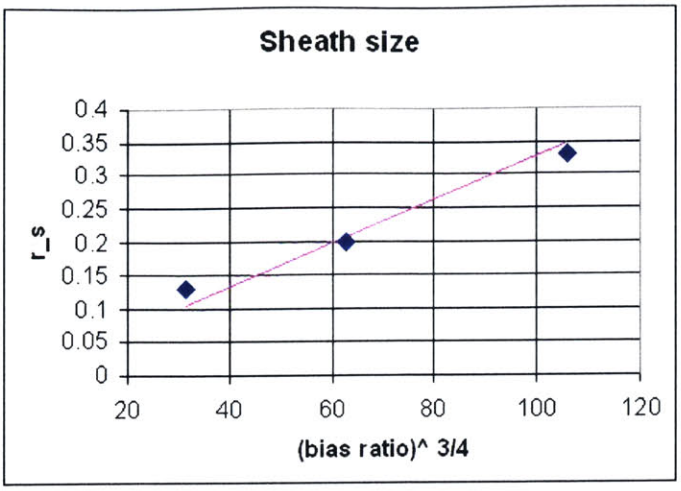

Figure 5-13: The dots represent the result obtained in the case $r_p = 1\lambda_D$ and the plain line shows a linear relation. r_s is given in meters

The only one noticeable difference is the dumping of the plasma oscillations. This can be observed on the current collection plot which is very flat, compared with the quasi-neutral condition. (see figure 5-14).

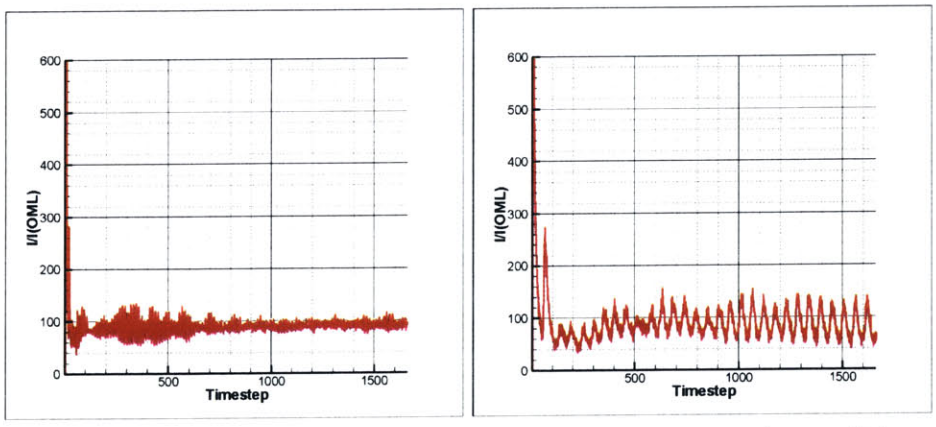

(a) $\phi_b = 0$ (b) ϕ_b from quasi neutrality-condition

Figure 5-14: Comparison between the collected currents for the case $r_p = 1\lambda_D$ and $\phi_p = 25V$ for two different boundary conditions

5.4.3 Relation between collected current and tether radius

In their work [2], Sanmartin and Estes computed the theoretical relation between the normalized collected current (I/I_{OML}) and the tether radius. A comparison between those values and the values obtained through the simulation is very satisfactory and show a very good match between the theoretical and numerical values. This is also to be related with the fact that for radii larger than $1\lambda_D$, the OML is not valid anymore, which leads to a significant decrease in the ratio I/I_{OML}.

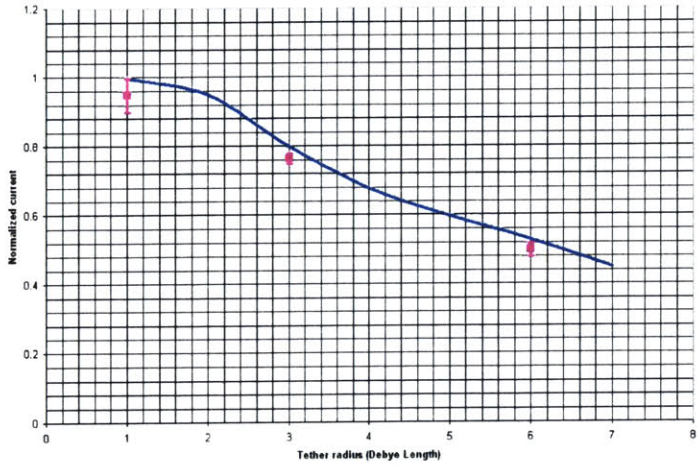

Figure 5-15: The plain line is the normalized current as predicted by Sanmartin and Estes [2], the error bars show the value obtained in the simulations

Chapter 6

Nominal case, with flow and magnetic field

6.1 Parameters

This nominal case is designed to represent the conditions of use of the tether. The plasma parameters are given in table 7. Concerning the tether parameters, they are

Plasma density	$10^{11}\ m^{-3}$
Plasma temperature	$1160\ K$
Electric charge	$1.6 \times 10^{-19}\ C$
Electron mass	$9.1 \times 10^{-29}\ kg$
Ion mass	$2.672 \times 10^{-25}\ kg$
Debye length	$7.440 \times 10^{-3}\ m$
Plasma time	$5.610 \times 10^{-11}\ s$
Flow velocity	$8000\ m.s^{-1}$
Magnetic field	$3 \times 10^{-5}\ H$

Table 6.1: Plasma parameters

the same as the ones of the symmetric case:

Radius	$1\lambda_D = 7.440 \times 10^{-3}\ m$
Potential	$25\ V$

Table 6.2: Tether parameters

6.2 Ion density

Ion density can be observed on figure 6.2.The ion density is strongly influenced by the meso-thermal condition. As a consequence, it shows a wake structure: ions are flowing toward the tether but they are slowed down and deflected due to the tether high potential. Then because of the structure of the potential itself, it is possible two make a distinction between two different parts. First of all there is a wake (see area A on figure 6.2) which is created because of the region in which the potential is so high that it is still coulombian ($\sim 4V$ on figure 6.4). In this region there are no ions at all. Indeed, depending on their energy, ions are either deflected or reflected (slow ions are deflected because they cannot go deep enough into the potential, whereas highly energetic ions are reflected when they finally encounter a very high potential) . Moreover it can be seen that the wake starts to close itself with an angle of the order of U/v_{Ti}.

Then it is possible to observe another wake structure, which is broader and less pronounced (see area B on figure 6.2). This wake structure comes from the magnetic wings of the potential. In this area, ions are slowed down and deflected. However, highly energetic ions are able to cross the potential and to go through it, at the cost of a part of their kinetic energy, which they recover after crossing the potential wings.

6.3 Electron density

Electron density can be observed on figure 6.3. Because of the tendency of the plasma to stay quasi-neutral on larger scales than the Debye length, the ion density plays a decisive role in the the distribution of the electron density. Indeed, the apparition of a wake in the electron density is not the consequence of the plasma flow itself but a consequence of the presence of a wake in the ion density. However, close to the tether, because of its high potential, quasi-neutrality is violated, and it is possible to observe the presence of a sheath with higher density of electrons.

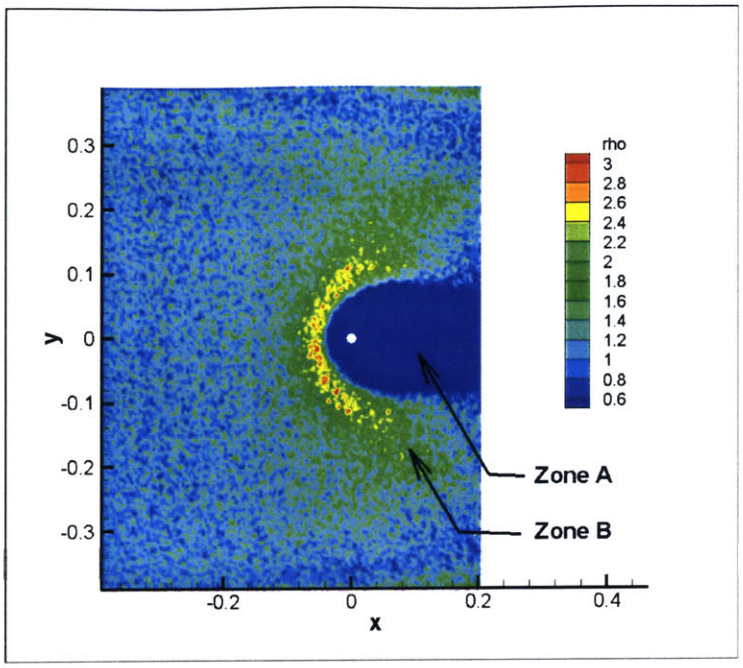

Figure 6-1: Ion density for a potential equal to 25 V. Distances are given in meters

.

It can also been noticed that as well as in the symetric case, the electron density goes through a minimum when it gets closer and closer to the tether.

6.4 Potential

The potential close to the tether is high enough, compared with the space charge effect to be axisymetric. However, for lower potentials, it is interesting to notice the occurence of two "wings". Those wings are due to the presence of the magnetic field. Indeed, because of the magnetic field, the motion of electrons is "contained" by the magnetic lines. Therefore, the positive potential also extends along those lines. On figure 6.4, it is clear that the wing are truncated by the boundary. However it occurs when the potential already reached a fairly low potential ($\sim 1V$).

The wing angle should be arctan $\frac{U}{v_{Te}}$. However U has been artificially increased, so the angle is exaggerated.

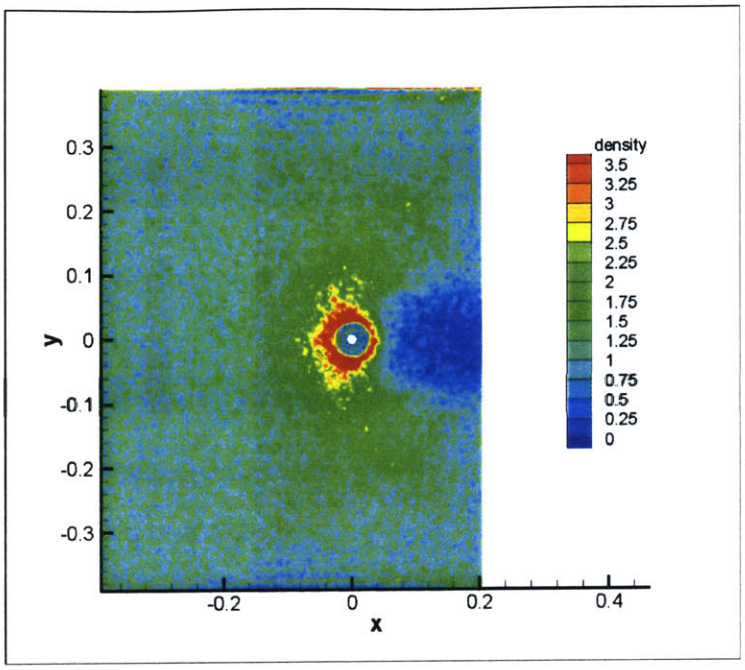

Figure 6-2: Electron density for a tether potential equal to 25 V

Finally the structure of the potential must be related to the ion potential. The first wake in the ion density is created by the coulombian and axi-symmetric part of the potential, up to voltages of the order of $5V$. Then the second part of the potential, the wings are responsible for the second wake structure of the ions.

6.5 Charge density

Quasi-neutrality stands almost everywhere in the model, except close to the tether. Close to it, its high voltage prohibits the presence of any ions. In the wake, because of the very low densities, quasi-neutrality is violated, and it can be seen that there are more electrons than ions there (due to the higher thermal velocity of electrons). And finally, on the side of the tether, where one can notice an accumulation of ions.

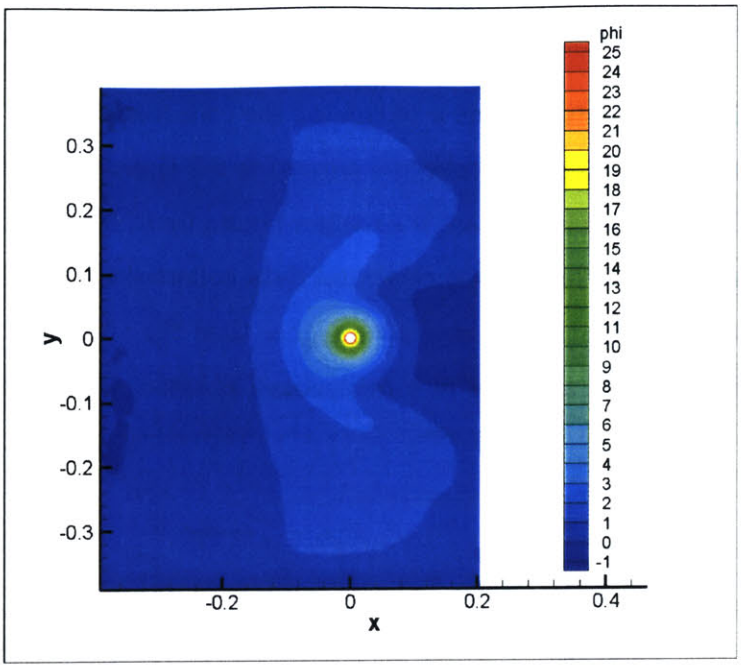

Figure 6-3: Potential for a tether potential equal to $25V$. Distances are given in meters

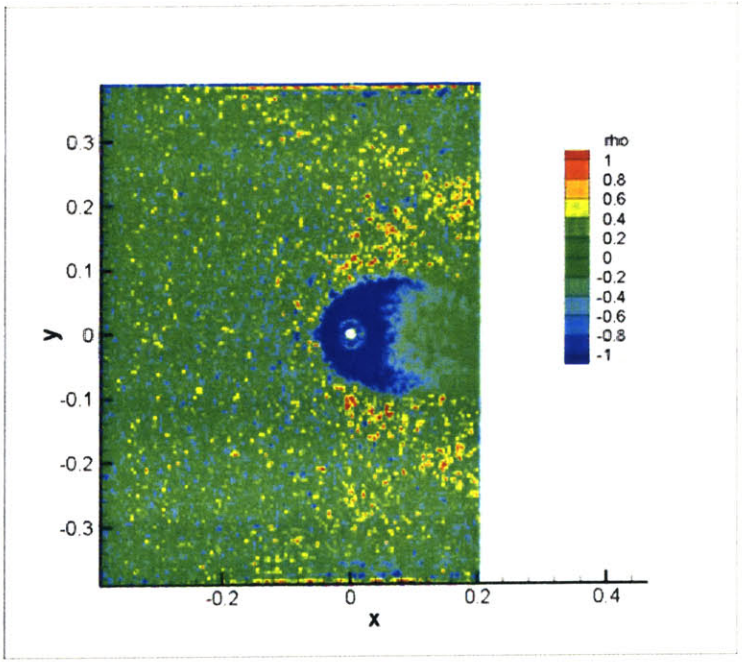

Figure 6-4: Charge density for a tether potential equal to 25 V. Distances are given in meters

6.6 Current collected

The goal of this work is to provide a model for the collected current. Moreover it is quite interesting to see that the collected current is 2.2 times higher than the OML current, which in the symmetric case is an upper bound limit. Those number were not completely unexpected. Indeed, experimental data collected during TSS-R2 showed that the actual collected current was much higher than the current predicted by the Parker-Murphy limit for a sphere in a magnetized plasma. On figure 6.6, collected

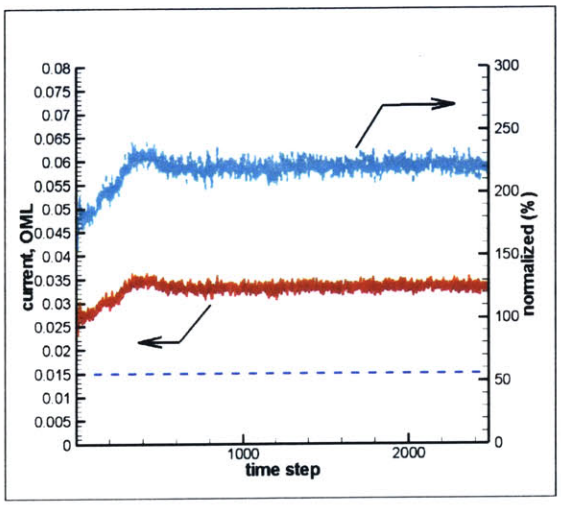

Figure 6-5: Current collected (% of OML) for a tether potential equal to $25V$. The light line represent the OML current percentage, the dark line represents the actual current $(A.m^{-2})$

current is the solid line, OML current is the straight dashed line. The light dotted line represents the current collected in OML percentage.

6.7 Validation of the "accelerated model"

In this section the author compares the results obtained from two different simulations: the simulation using original mass m_i for ions and original velocity U for the tether, and the one using m_i/α^2 as the ion mass and αU as the tether orbital velocity. (see section 3.3.2). In order to be able to make the comparison, results obtained by Onishi in his PhD thesis work were used. The output we obtained from the accel-

erated simulation were very similar to the standard ones for all the parameters: ion and electron density, electric potential and collected current.

Onishi results are presented below: However, in the "accelerated model" the non-

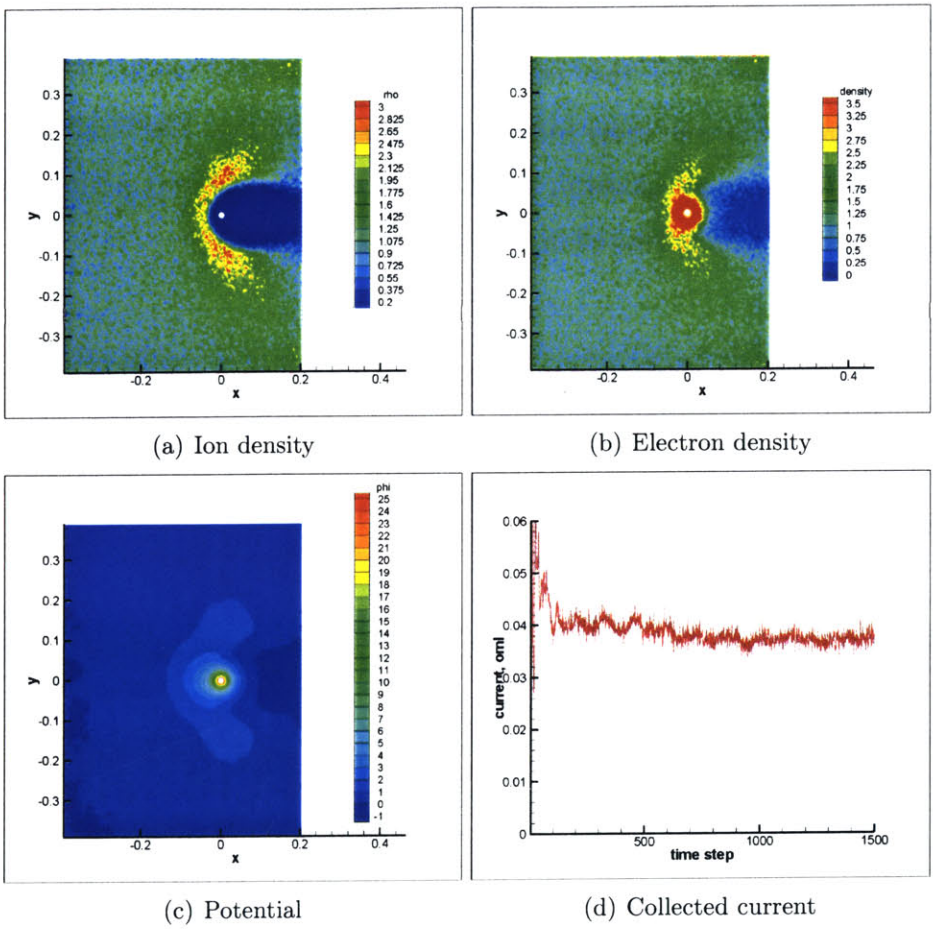

(a) Ion density

(b) Electron density

(c) Potential

(d) Collected current

Figure 6-6: Tether potential equal to 25 V, real ion mass and real orbital velocity. Distances are in meters and all densities are normalized by n_∞

dimensional quantity $\frac{1}{2}m_eU^2/kT$ is not conserved. This has almost no impact on the simulation. But it probably affects a little bit the wake region. Indeed this is the region where this ratio is important and by being 5 times higher, it makes it more difficult for the electrons to enter the wake.

6.8 Discussion

In this section we discuss the physics of the situation. Because of the magnetic field, electrons are contained on the magnetic lines. This enable the potential to widely extend in the magnetic direction. In a steady case, one would have expect them to extend up to infinity. However in this case, when the ram energy of ions becomes of the order of the potential, they can penetrate the potential wings. Then electrons have to follow the ions in order to maintain quasi-neutrality. The final result is that even magnetic wings get shielded, which allows the ions to wrap around the tether, creating the structure presented in section 6.2.

Chapter 7

Results and Interpretation of the flow case for $\phi_p = 50V$

The simulation was then ran for another set of conditions. Essentially the potential of the tether was increased to $50V$. Then, in order to be able to capture the physics, the size of the domain was laterally increased by a 1.5 factor.

Plasma density	$10^{11}\ m^{-3}$
Plasma temperature	$1160\ K$
Electric charge	$1.6 \times 10^{-19}\ C$
Electron mass	$9.1 \times 10^{-29}\ kg$
Ion mass	$2.672 \times 10^{-25}\ kg$
Debye length	$7.440 \times 10^{-3}\ m$
Plasma time	$5.610 \times 10^{-11}\ s$
Flow velocity	$8000\ m.s^{-1}$
Magnetic field	$3 \times 10^{-5}\ H$

Table 7.1: Plasma parameters

Radius	$1\lambda_D = 7.440 \times 10^{-3}\ m$
Potential	$50\ V$

Table 7.2: Tether parameters

Then a comparison with the 25 V case can be made.

7.1 Potential

The increase in the tether potential makes a very significant difference in the overall potential of the domain. First of all the coulombian part of the potential is now bigger. In addition, the magnetic wings are now much wider in the magnetic field direction. This extension of the magnetic wings is what actually make it difficult to run simulations for higher voltages: they are the reason why the computational domain needed to be extended in the **B** direction.

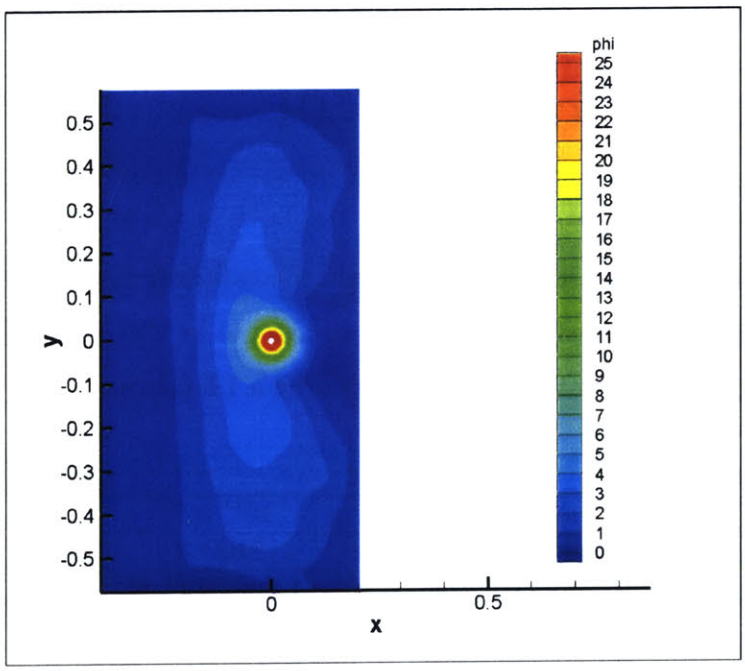

Figure 7-1: Electric potential ($\phi_p = 50V$). Distances are given in meters

7.2 Ion density

Because of the change in the potential, ion density is also affected. The wake is now bigger. However each component of the wake is changed in a different way. The primary wake size changed in proportion with the tether potential. This is due to the fact that the maximum of ion density is located where potential energy is equal to kinetic energy.

The second part of the wake, wider, is due to the magnetic wings. Since those are now much wider, this magnetic wake is also much more diffuse. It is to be noticed that the change in its shape, is not similar to the change in the primary wake. Indeed here the potential structure is not only broader, but it extended in the magnetic field direction.

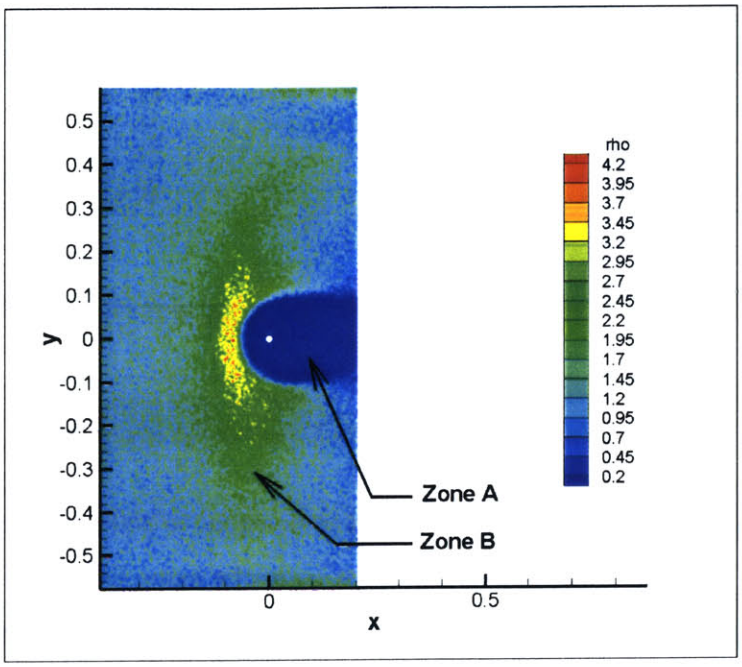

Figure 7-2: Normalized ion density ($\phi_p = 50V$)

7.3 Electron density

As observed in the nominal case, electron density is driven by the ion density, except in the sheath. However in this case, one can notice the occurrence of waves on the lateral boundaries of the computational domain. Those wave are created by the boundary conditions, and could be responsible of the oscillations that can be observed while the simulation is running.

In order to investigate more in detail this phenomenon, two probes were set up to measure the electron density close to the boundary (at locations $x = 0m, y_1 = 0.55m, y_2 = 0.5m$, see figure 7.3). Thus, the propagation of a wave could be estab-

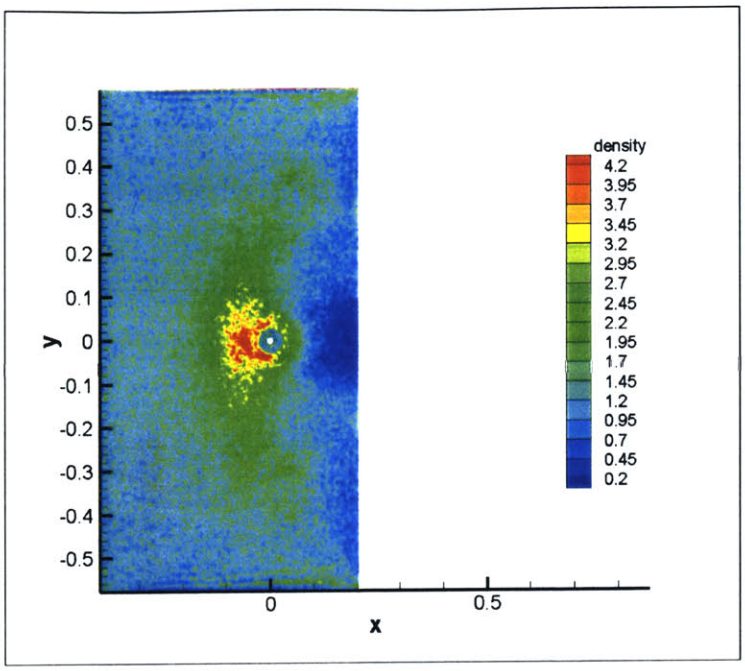

Figure 7-3: Normalized electron density ($\phi_p = 50V$)

lished (see figure 7.3). Its period was found to be equal to 250 time-steps, which gives $T = 25\tau_P$. The fact that these oscillations have the same frequency as the oscillations of the current collection indicates clearly their relation. In addition it could be established that the propagation velocity was equal to $\sim 9 \times 10^5 m.s^{-1}$ this velocity is actually very close to the electron thermal velocity: $v_{Te} = 1.32 \times 10^5 m.s^{-1}$. That gives an indication of the fact that those waves are actually clusters of electrons which were injected in a non-continuous manner.

7.4 Current collection

Once again, the collected current is very important, since it is the key parameter in use of Electrodynamic space tethers. In the $50V$ case, we will do two main observation. First of all, contrary to the symmetric case, we can see that the tether potential plays an important role. Indeed, whereas for the $25V$ case, the ratio I/I_{OML} was almost equal to 2.2, in the $50V$ case we have a ratio equal to 1.6 (see figure 7.4). Thus one can observe that collected currents are equal in both cases, although the OML

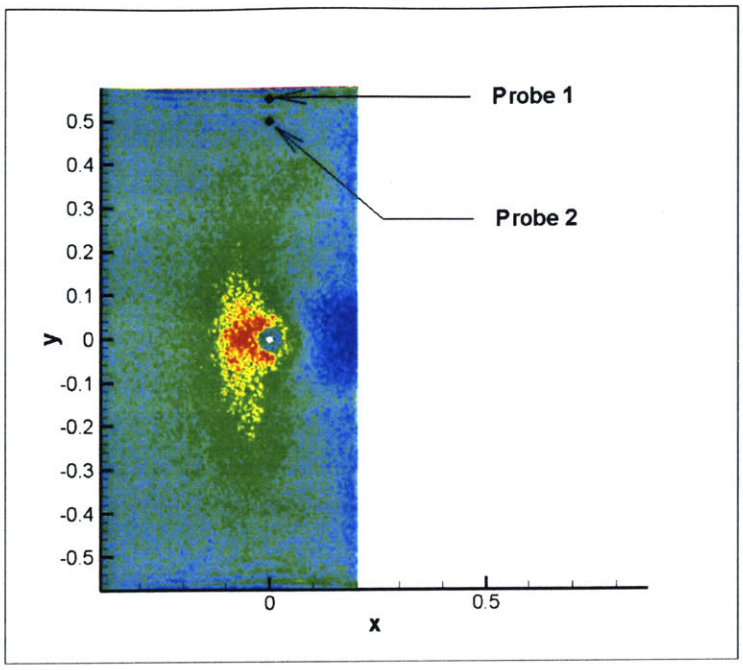

Figure 7-4: Location of the two probes used for the investigation of oscillations. Distances are in meters

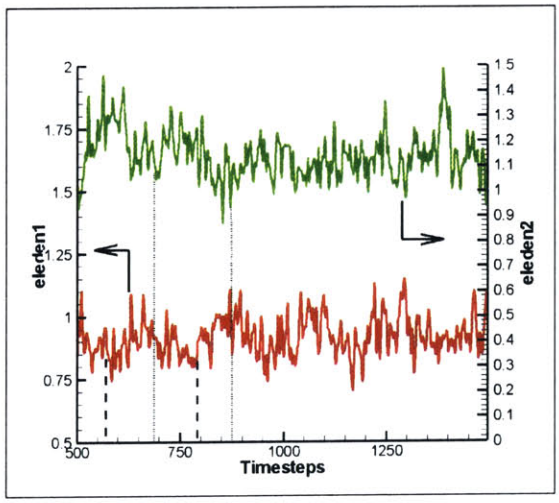

Figure 7-5: Normalized density measured at the probes

current is equal to 0.015 $A.m^{-2}$ in the $\phi_p = 25V$ case, and equal to 0.021 $A.m^{-2}$ in the $\phi_p = 50V$ case.

The second observation that one can make is the oscillations in this collected current. Those occur with a regular periodicity: $\sim 250 timesteps = 25T_p$. Those oscillations

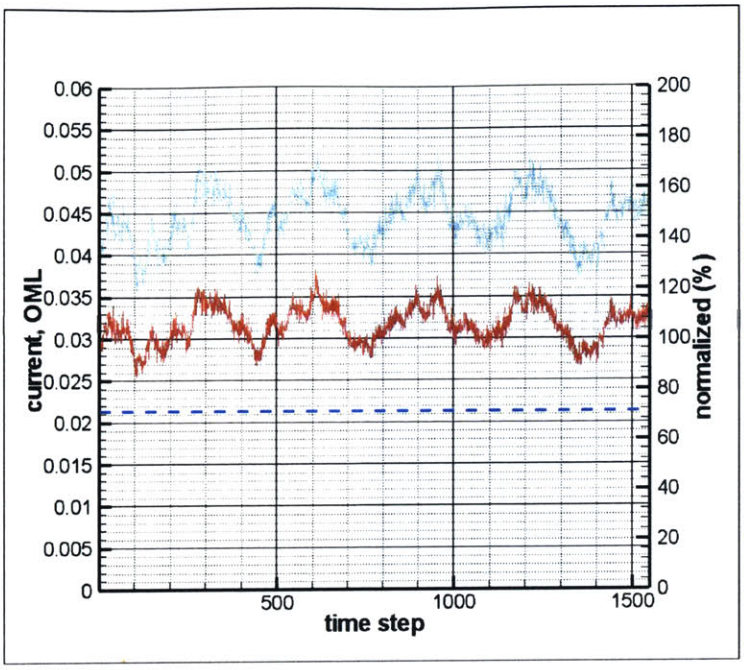

Figure 7-6: Collected current ($\phi_p = 50V$), the light line represents the percentage of OML current, the dark line represents the actual current ($A.m^{-2}$)

are a consequence of the waves created at the boundary condition, during the electron injection process: clusters of electrons are injected and when they reach the tether, they increase the amount of collected current.

Chapter 8

Conclusion and recommendations

8.1 Summary

An existing model has been upgraded in order to investigate the physics of current collection by electrodynamic space tethers at high voltages. This model is based on PIC code and description of it can be found in Appendix A.
This model allowed the author to study two main cases: a quiescent and a flowing plasma. In the study of the quiescent plasma several important results were obtained:

- The current collection was compared with theoretical existing models, and its correlation with tether bias and tether radius was proved to match with these theoretical models.

- The electron density could be accurately studied, which confirmed the existence of a minimum in the sheath region. This minimum had been predicted by Sanmartin and Estes.

- Some phenomena like the oscillation in the collected current still have to be explained.

In the flowing case, it was possible to reach a tether voltage equal to $50V$ (equivalent to $e\phi/kT_e = 500$, which is twice the voltage which could be reached by T. Onishi.

This was made possible by a larger grid and a better understanding of the transients at the starting of the simulation. The following results were obtained:

- The collected current was found to be higher than OML, as in T. Onishi's work.
- The electron density was found to present a minimum, as well as in the symmetric case.
- The structure of the potential was found to extend widely in the magnetic field direction when the tether potential is increased. The computation resolves only the near-zone of these "wings", but probably far enough, since the wing potential at the boundary is far belo the ion ram energy.

8.2 Future work

The following steps still need to be done:

- A deeper investigation on the boundary conditions, which are still not clear, is needed. Especially in the presence of a magnetic field.
- The simulations could be realized on a new domain which would be the upper half of the present domain. This way, by implementing a symmetric boundary condition, one could extend the computational domain much further from the tether at no computational cost.
- The previous observation would make it possible to implement a better modeling of the boundary conditions which would be closer to infinity.

Appendix A

Description of the code

The code used in this thesis was a PIC (Particle-In-Cell) code. Applied on a rectangular domain, with a quadrilateral grid. The author intends here to explore more in detail each step of the computation.

A.1 Flow Chart

The program is organized in several steps. First of all, the grid is generated. It is a structured grid, generated by a Poisson grid generator. Then, all the constants of the problem are initialized, and the initial condition are generated.
The next step is the loop on time iterations: spatial charge is assigned to the nodes of the grid, a Poisson solver solve the equation giving the potential. From this potential, the electric field is simply computed by differentiation. Finally this electric field, combined with the magnetic field, allows to solve the equations of motion (by two successive integrations) and compute the new position of particles. This closes the loop.

A.2 Preprocessing

The preprocessing includes three different steps. The first one is the generation of the grid. Then comes the precalculation of tables of integrals. Finally position and

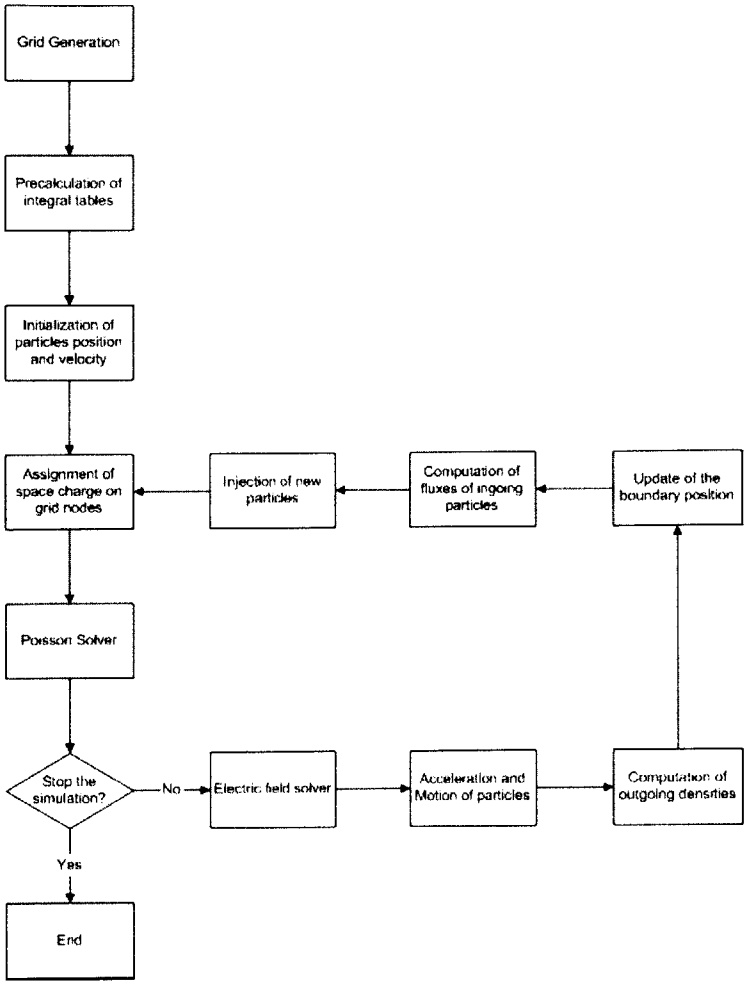

Figure A-1: Flow Chart of the PIC code used in this thesis

velocity of ions and electrons are initialized, as well as the boundary condition of the potential.

A.2.1 Grid generation

The choice of a rectangular domain here results from the desire to be able to easily increase the size of the computational domain. Indeed, in the early time of this code, a circular domain had be chosen, but the trouble was that for a large domain, cells tend to get bigger and bigger, or to be very stretched. Moreover large cells require large number of particles for a good statistics

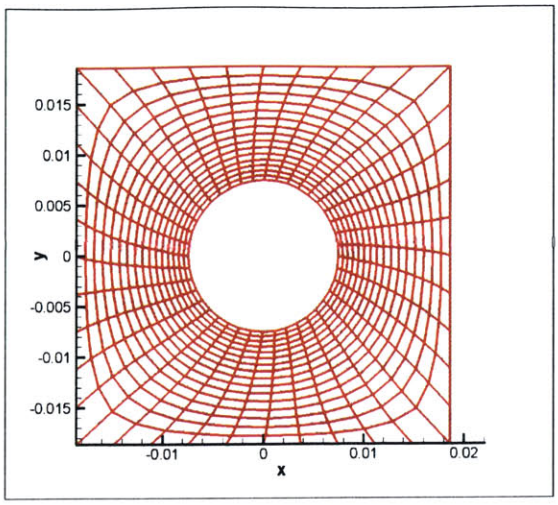

Figure A-2: Grid in the vicinity of the tether, distances in meters

However, the tether we study being circular, at some point it is necessary to include a "non-rectangular grid". In order to generate this grid we use a Poisson grid generator. The size of the cell is chosen so that we can keep a good accuracy. As a consequence, in order to be able to capture the physics of our plasma, we should use a grid resolution smaller than the Debye length. We actually decided to go for a size of the cell equal to $\lambda_D/2$. This is the exact size of the rectangular cells, but cells are of course smaller close to the tether, due to the grid deformations.

A.2.2 Pre-computation of integral tables

Several times in the code execution, complex integrals need to be calculated. Those multiple integrals cannot but computed analytically and therefore they need to be computed numerically. However those computations are extremely time demanding and most of the time they need to be repeated many times (in the case of the motion of electrons in the analytical domain for example, they need to be computed several thousands of time). That's why, instead of computing those integral during the code execution, they are pre-calculated, for given series of values, which are chosen in order to cover all the values actually needed. Then when values are needed, they are linearly interpolated from the table values.

Those precalculated integrals fall into two categories: integrals related to the motion of electrons in the analytical domain (corresponding to equations given in section 3.2), and integrals related to the injection of new particles (corresponding to equations given in section 3.3.2). The first ones are actually more complex in the sense that they are functions of several parameters (Energy, Angular Momentum, Potential and Radius) whereas the latter depend only on the potential at the boundary. This is why they are separated into two different programs: it is much faster to compute tables for injection than tables for analytical motion. As a consequence, one want to be able to compute them separately.

Finally the method use to compute those integral is a very simple Riemann integration by rectangle method. (This can actually be changed very easily into a trapezoidal method which is much more accurate for the same amount of computational time).

A.2.3 Initial conditions

Before starting the iterations, it is important to generate the initial conditions of the model. This means initializing position and velocity of each particle, and initializing the boundary condition.

Starting from scratch, no-flow case

In the case of the No-Flow problem, starting from scratch is usually the chosen solution. Indeed, in this case, ions and electrons are set to have the same mass, and therefore it is quite fast to get a good pattern for the densities of ions and electrons as well as for the potential.

In this case, the initialization of ions and electrons is very simple: electrons are randomly and uniformly distributed all over the computational domain, the only one condition being for them to have an overall density equal to their density at infinity (n_∞). Then they are assigned a random velocity, following a Boltzman distribution (as a consequence their average velocity is v_T^e).

Then the ions are distributed using the following method: same position as the elec-

trons, but random velocity (once again using a Boltzman distribution but this time centered on v_T^i).

The last step is to initialize the potential on the boundary. Since the domain is fairly large, boundaries are very far from the tether, whose potential is fixed. Therefore it is assumed that a boundary potential equal to 0V is a good initial estimate.

Starting from an existing profile, flow case

In the flow and magnetic field case, because of the slowness of the ions, it is important to start from a configuration close to the one expected. Therefore, instead of starting from scratch, one can start from an existing file, by turning the switches `reread` and `reread-phi` on. This way electrons and ions will be set up with a distribution close to the final one, greatly reducing the computational time.

Moreover, because of the finiteness of the domain, it is necessary at the beginning of the simulation to start with a different boundary condition than the one applied at the end. If not then it is impossible to get rid of the potential wall that creates naturally at the beginning. In order to avoid it, one should run the simulations normally except for the Poisson solver, in which the potential boundary condition should be zero. (That can be done by switching the value of the potential on the boundary to zero after having calculated the values of fluxes of incoming particles). It was actually impossible to start from scratch without using the previous method for tether voltages higher than $25V$.

Starting from scratch, flow case

In the flow case, when starting from scratch, it takes a very long time for the simulation to reach the expected pattern. That is why in this case, one might want to use a purely mathematical trick, which is to use two different times, one for the ions and one for the electrons, the one for the ions being much faster than the one from the electron. Typically what the author used was a ratio of 10: $dt_i = 10dt_e$. This way the wake is going to create itself much faster. Then, once one gets a good "profile", he can just stop the simulation, reset the two times to be equal, and restart a new

simulation using the previous result as his initial condition.

A.3 Assignment of space charge

Once all the particles have been generated, the iterations on time can start. The first step of those iterations is the assignment of space charge.

The space charged is assigned to each grid node through a linear interpolation process, using area weighting functions. This process is very well explained in Onishi's master thesis. That is why we will go very fast here in the explanation of the process, through a quick example.

Let consider a super-particle of charge q located at (x, y), and let consider that this super particle is located between the following grid nodes: $N_{i,j}, N_{i+1,j}, N_{i,j+1}, N_{i+1,j+1}$, with coordinates:$(x_i, y_j), (x_{i+1}, y_j), (x_i, y_{j+1}), (x_{i+1}, y_{j+1})$. Then the space charge is assigned using the following method: first the charge density ρ is calculated:

$$\rho = \frac{q}{(x_{i+1} - x_i)(y_{j+1} - y_j)} \tag{A.1}$$

Then this charge density is affected to each node by multiplying it by a corrective factor. This factor is equal to the ratio of the area of the rectangle whose vertices are the super particle and the opposite node over the area of the whole cell. This gives for example for the node $N_{i,j}$:

$$\begin{aligned} \rho_{i,i} &= \rho \times \frac{(x_{i+1} - x)(y_{j+1} - y)}{(x_{i+1} - x_i)(y_{j+1} - y_j)} \\ &= q \times \frac{(x_{i+1} - x)(y_{j+1} - y)}{[(x_{i+1} - x_i)(y_{j+1} - y_j)]^2} \end{aligned} \tag{A.2}$$

An illustration of this example is given on figure ??, where node A is what we called node $N_{i,j}$ This method gives a second order accuracy as long as the grid is rectangular and uniform (i.e. an error of the order $O(\delta x^2 \delta y^2)$. In our case, in the area close to the tether, the grid is no longer uniform. However, because we are never confronted with a situation where two adjacent cells have a very significant difference in size and

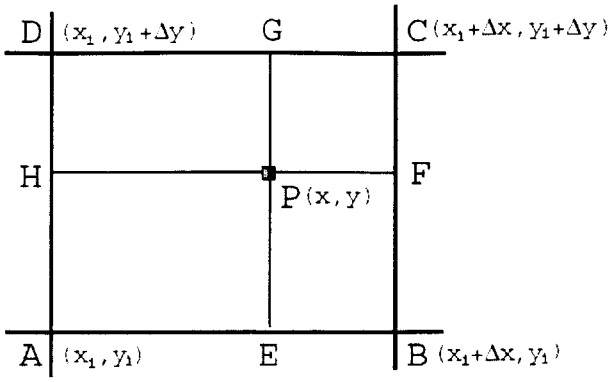

Figure A-3: A uniform rectangular grid - Here we get for node A: $\rho_A = \rho \times \frac{[PFCG]}{[ABCD]}$

shape, we can consider that we are close enough to second order accuracy.

A.4 Poisson Solver

Once the space charge has been interpolated to grid nodes, it is possible to solve the Poisson equation:

$$\triangle\phi = -\frac{\rho}{\epsilon_0} \tag{A.3}$$

This done by using an over-relaxation Poisson solver, called SLOR in the literature. A description of this solver can be found in numerical recipes for FORTRAN. The coefficients needed in order to take into account the deformation of the grid while using the solver are actually computed in the grid generation phase.

A.5 Computation of the electric field

The electric field is derived by simple differentiation of the potential.

$$\mathbf{E} = -\nabla\phi \tag{A.4}$$

This is done very easily because of the uniformity of the grid. In the non-uniform grid domain however this calculation would have been difficult. But, the non-uniform

grid region is inside the analytical domain. Therefore we are insured that the electric field will never been calculated there.

A.6 Acceleration and motion of electrons

We must make a distinction between two different cases: electrons which are far enough from the tether to be in the numerical domain, and electrons that are in the analytical domain.

A.6.1 Numerical domain

In this case we use a standard PIC method. First of all, the electric force on the particle is computed as follow: the electric field is interpolated from the grid nodes to the particle. This is done using the same method, but in reverse, as the one used for the assignment of space charge on the node. Then we know that we have:

$$\mathbf{F_E} = q\mathbf{E} \tag{A.5}$$

Once this electric force as been calculated, we can accelerate each particle by combining the effect of electric and magnetic field. Since the magnetic force is highly dependant on the velocity vector of particles, we used the following method to compute the new velocity:

$$\begin{aligned} \mathbf{v_{n+1/3}} &= \mathbf{v_n} + \frac{1}{2}\frac{q}{m}\mathbf{E}dt \\ \mathbf{v_{n+2/3}} &= \mathbf{v_{n+1/3}} + \frac{q}{m}\mathbf{v_{n+1/3}} \times \mathbf{B}dt \\ \mathbf{v_{n+1}} &= \mathbf{v_{n+2/3}} + \frac{1}{2}\frac{q}{m}\mathbf{E}dt \end{aligned} \tag{A.6}$$

The magnetic force is computed in the middle of the acceleration due to the electric field. Once the new velocity is known, it is possible to get the new position of particles, by integration:

$$\mathbf{x_{n+1}} = \mathbf{x_n} + \mathbf{v_{n+1}}dt \tag{A.7}$$

In order to keep a good precision, if the travel distance of an electron was found to be too big (typically more than one Debye length), sub-cycling is introduced: instead of having one time-step dt, the time-step is divided in smaller time-steps, and the motion is calculated in smaller jumps. And, at each of the new position, the electric field is recalculated.

A.6.2 Analytical domain

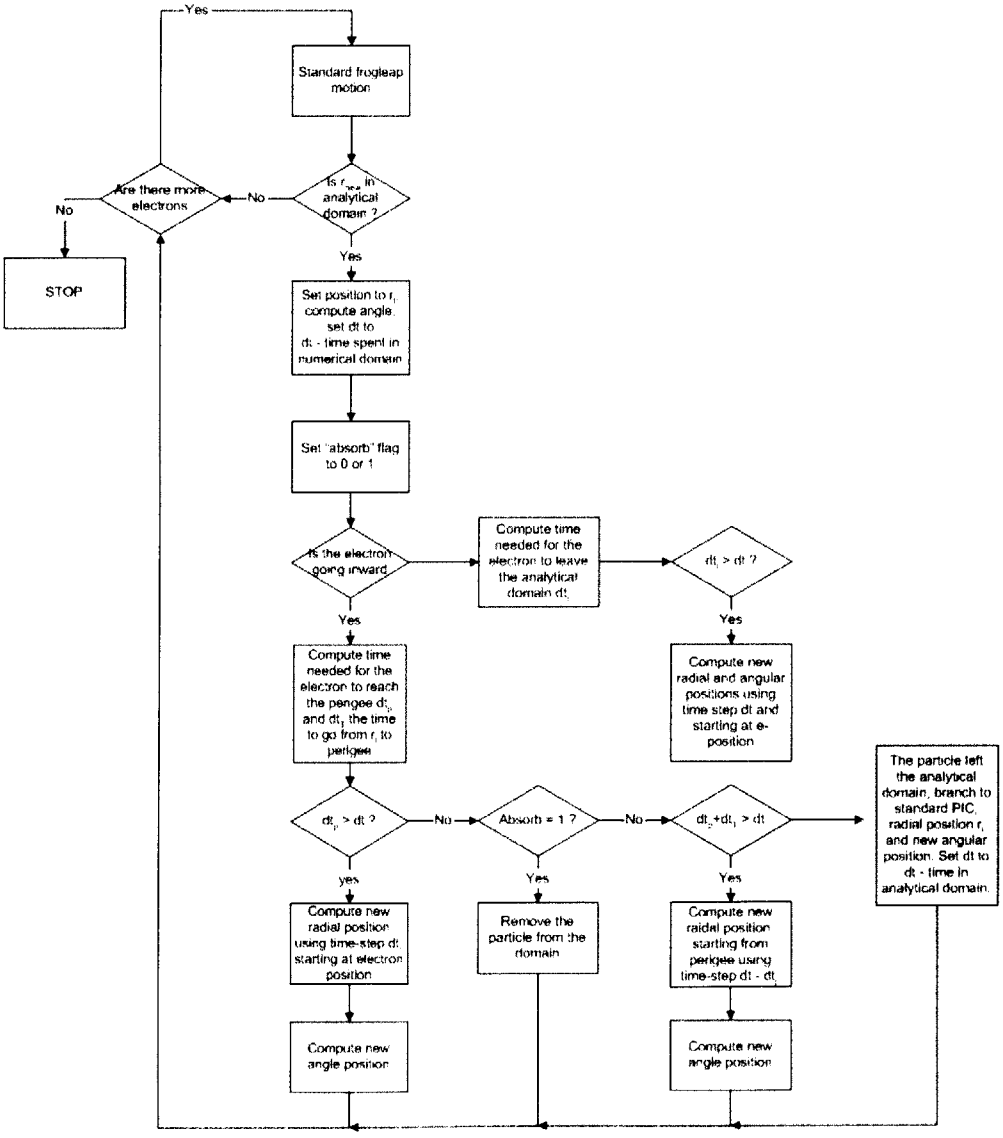

Figure A-4: Description of the motion of an electron

For particles close to the tether, the motion is computed analytically. The method used is described in section 3.2. That is why here we will only go through the details of the program. Figure A-4 shows a flow chart of the motion of electrons and more particularly the analytical motion.
First of all let consider an electron which is inside the analytical domain at the beginning of the iteration (corresponding to $r \leq r_l$), and that will stay in the analytical domain for the whole time-step.

- The first step of the algorithm is to compute what will be the periapse of a given electron. If the periapse is found to be lower than the probe radius, then a flag ("absorb") is set on value 1: this means that this particular electron is going to be absorbed by the tether. Otherwise the flag stays equal to zero.

- Then the program checks if the particle is going inwards or outwards: If the particle is going inwards, then it computes how long it is going to take for the electron to go from its position to its periapse.

  - If the time required is greater than onetime-step, the we know that the electron will not reach its periapse during this time-step. Therefore we just need to compute the the new angle of its position and from this its new radial distance to the tether.

  - If the time required to go to the tether is lower than one time-step, then we know that the particle is going either to be absorbed or to pass the periapse. If it was absorbed, it just need to be removed from the domain, and be added to the collected particles list. If not, then we have to check if it went out of the analytical domain or not. This is done by considering wether the time required to go from the particle position to the exit point of the particle is greater or lower than the time-step.

    * If it stayed in the analytical domain, we can compute the new position of the electron by simply considering that the electron actually started

from its periapse, and by reducing the length of the time-step by the corresponding time.

  * If the electron exited the analytical domain, it goes back to the standard frog-leap motion, with as a new position its exiting position. In addition the time-step length is reduced by the corresponding time.

- If the particle is going outwards, then we know that the particle already passed its periapse. We can calculate how long it would take for the particle to exit the analytical domain. If this time is longer than the time-step, we know that the particle is going to stay. Otherwise, the electron will leave.

  - If the particle stays we can easily compute its new coordinates.
  - If the particle leaves the analytical domain, we send it back to the standard frog-leap method, but with a starting point located at its exiting point, and the time-step duration is reduced by the corresponding time.

A.7 Computation of outgoing densities

This is directly adapted from Onishi 2002 [5].
The density of outgoing electrons is derived by considering the ougoing flux of particles for which the expression is:

$$\Gamma_e = n_e v_e \tag{A.8}$$

where v_e^{out} is the flow velocity due to the outgoing electrons, that is, the average velocity normal to the boundary, which is calculated computationally as follows, during the period of one time-step dt, sampling all particles which go through the boundary cell surface (which has a width dx but is later taken to the limit $dx \to 0$) leads to particles flux distribution function $wf(w)$. In order to derive a distribution function, we need to sample particles at an arbitrary moment during this time step. To do so, we consider the "probability" that a particle is on the boundary at the arbitrary moment during the time-step dt. For brevity, all particle velocities, denoted by w_i

$(i = 1 \sim k)$, have been projected on the normal to the surface ($w_i = \mathbf{w_i}\dot{\mathbf{n}}$). One particle which travels through the surface with a velocity wi has the probability of being on the surface as dx=widt. It can be also interpreted that there is a fraction "$dx/w_i dt$" ($\ll 1$) of all the crossing particles on the boundary at the moment. Therefore the average velocity is given by:

$$\begin{aligned} \bar{v} &= \frac{\sum^k \frac{dx}{w_i dt} w_i}{\sum^k \frac{dx}{w_i dt}} \\ &= \frac{k}{\sum^k \frac{1}{w_i}} \end{aligned} \tag{A.9}$$

which is independent of dx. Trivially, we can take the limit of $dx \to 0$. Substituting the average velocity A.9 and $\Gamma = kdtdS$ into:

$$n_e^{out} = \frac{k}{\bar{v}dtdS} \tag{A.10}$$

we get the density of outgoing particles.

$$n_e^{out} = \frac{\sum^k \frac{1}{w_i}}{dtdS} \tag{A.11}$$

where dt is the time-step and dS is the area of the outside boundary.

A.8 Computation of boundary condition

Once we have computed the density of outgoing particles, the value of the potential at the boundary can be determined using the outgoing densities, numerically computed, and the ingoing densities, analytically computed and ϕ-dependant. This is done by a bisection method whose description can be found in "Numerical Recipes" [7], applied to the quasi-neutrality equation:

$$n_e^{in}(\phi_b) + n_e^{out} = n_i^{in}(\phi_b) + n_i^{out} \tag{A.12}$$

From the value of ϕ_b it is now possible to compute the fluxes of incoming particles, ions and electrons. Indeed those fluxes where precalculated and stored into tables during the initialization phase.

A.9 Injection of new particles

When the potential and the fluxes at the boundary have been calculated, it is possible to inject new particles. The number of particles to be injected is obtained as follow:

$$k = [\Gamma dt dS] \tag{A.13}$$

Then electrons and ions are randomly injected using a Maxwellian distribution for their velocity, and a uniform distribution for their location. The method used to implement those distribution is a rejection method (see "Numerical Recipes" [7] for further detail).

Appendix B

Program, subroutines and variables

The program we used in this thesis was coded in FORTRAN 77. This appendix can be considered as a comment of this code. Combined with appendix A, it can be used as a User Manual for the program

B.1 Programs

The project in itself contains actually four different programs. The first one is `input.f`. This program generate the grid and the physical parameters. Its output is a file called `input.dat`. This program should always be compiled and run first. Indeed it generates all the constants needed.
Then, programs `new_dens.f` and `new_gamm.f` should be number two on the list. They compute the densities and fluxes of incoming particles, in the form of tables. The varying parameter of those table is the potential at the boundary ϕ_b.
Finally, the main program is `ngfmag.f` which is the actual simulation. Its outputs are various plots, whose format is Tecplot (.plt files).

B.2 Subroutines

The main program `ngfmag.f` falls into several subroutines, called successively during the execution.

The first subroutines that are called are gathered in the file `precal.f`. They consist in the precalculation of tables for the various integrals used for the articles motion i.e. `rm_precal, dthetam_precal, dtm_precal`, as well as some table used for ions injection. This file also contains subroutine `electron_init` which initializes the electrons in the domain.
Then come subroutines of file `sub.f`. First of all, subroutine `asgn`. This subroutine is in charge of the interpolation of space charge related to electrons on the grid nodes. Then subroutine `asgn_i` doe the same but for the ions.
The subroutine `poisson` is the subroutine in charge of solving the poisson equation for the potential, whereas subroutine `e_field` differentiate the potential in order to get the electric field.
Then come the subroutine `move_accel` which is in charge of integrating the motion of electrons and ions. It starts first with the electrons, numerical and analytical motion, and then move the ions.
This is followed by the "boundary" subroutines:subroutine `neout_niout`, which computes the densities of outgoing particles, both ions and electrons ; subroutine `quasi_neutral`, which computes the potential at the boundary of the domain ; subroutine `gamma_flux`, which computes the values of fluxes of incoming particles, and finally subroutine `injection` which inject the new particles, ions and electrons.
Subroutines of the file `output.f` are the subroutines that produce plots. Each of those subroutines start with the prefix `op_` which make them easy to recognize.

B.3 Main variables

This program use many variables. Among those, many are very important. That is why they are described below.

B.3.1 Parameters

Among the parameters, the author wants to emphasize the following ones:

- `n_par` or `n_parc` represents the maximum number of articles in the domain.

- Constants characterizing the grid size are: `npc` is the number of grid nodes, `ncc` is the number of cells ; `nc_input1c, nc_input2c`, etc... represent the number of cells on each side of the domain (see figure B.3.1)

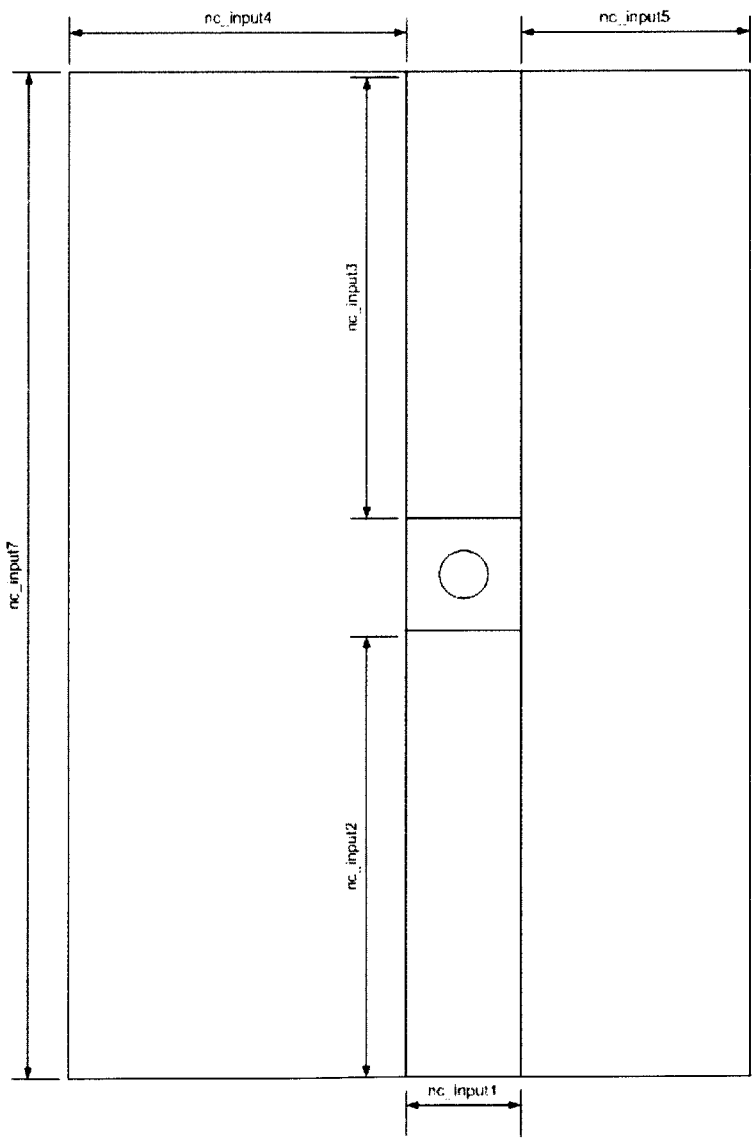

Figure B-1: Grid parameters

B.3.2 Particle variables

The information concerning particles is gathered in big arrays, whose size is `n_parc`. For the electrons we get: `x(n_parc)`, `y(n_parc)` for the position, and for velocities `vx(n_parc)`, `vy(n_parc)`. `ang_p(n_parc)`, and `tene(n_parc)` give namely the angular momentum and the total energy of electrons in the analytical domain. `phi_lp(n_parc)` gives the potential at the boundary of the analytical domain when the electron entered it.
For the ions we have: `xi(n_parc)`, `yi(n_parc)` for the positions, and `vxi(n_parc)`, `vyi(n_parc)` for the velocities.

B.3.3 Grid quantities

Quantities like potential or charge density are computed at grid points. They are given by the following arrays: `phi(npc)` and `rho(npc)`.
On the boundary, one have the following: `phi_b(nc_input8c)` and `phi_bave(nc_input8c)` are the values of the potential on the boundary of the analytical domain (the second one can be time averaged if wanted). Then one have `gammae(nc_input8c)` and `gammai(nc_input8c)` for the fluxes of electrons and ions.

Bibliography

[1] R.D. Estes J.R. Sanmartín. The orbital-motion-limited regime of cylindrical Langmuir probes. Phys. Plasmas 6 395, October 1999.

[2] R.D. Estes J.R. Sanmartín. The orbital-motion-limited regime of cylindrical langmuir probes. Phys. Plasmas 7 4320, June 2000.

[3] James G. Laframboise. Theory of spherical and cylindrical Langmuir probes in a collisionless, maxwellian plasma at rest. UTIAS report no. 100, June 1966.

[4] Tatsuo Onishi. Electron current collection by an electrodynamic bare tether in a quiescent unmagnetized plasma. Master's thesis, MIT, June 1998.

[5] Tatsuo Onishi. Numerical study of current collection by an orbiting bare tether. PhD thesis, MIT, August 2002.

[6] J.R. Sanmartín. Note on minimum of electron density inside the sheath (no flow, $r = r_{max}$). Unpublished.

[7] W.T. Vetterling B.P. Flannery W. H. Press, S.A. Teukolsky. Numerical recipes in Fortran 77, the art of scientific computing. 2nd ed.